Food and Chemical Toxicology 184 (2024) 114423

Contents lists available at ScienceDirect

Food and Chemical Toxicology

journal homepage: www.elsevier.com/locate/foodchemtox

Influence of artificial digestion on characteristics and intestinal cellular effects of micro-, submicro- and nanoplastics

Maxi B. Paul [a], Linda Böhmert [a], Andreas F. Thünemann [b], Katrin Loeschner [c], Lucas Givelet [c], Christoph Fahrenson [d], Albert Braeuning [a], Holger Sieg [a,*]

[a] German Federal Institute for Risk Assessment, Department of Food Safety, Max-Dohrn-Str. 8-10, 10589, Berlin, Germany
[b] Federal Institute for Materials Research and Testing (BAM), Division Synthesis and Scattering of Nanostructured Materials, Unter Den Eichen 87, 12205, Berlin, Germany
[c] Technical University of Denmark, Research Group for Analytical Food Chemistry, Kemitorvet 201, 2800, Kgs. Lyngby, Denmark
[d] Technical University of Berlin, Center for Electron Microscopy (ZELMI), Straße des 17. Juni 135, 10623, Berlin, Germany

ARTICLE INFO

Handling Editor: Dr. Bryan Delaney

Keywords:
Microplastics
Nanoplastics
Oral uptake
Artificial digestion
Gastrointestinal barrier

ABSTRACT

The production of plastics is rising since they have been invented. Micro, submicro- and nanoplastics are produced intentionally or generated by environmental processes, and constitute ubiquitous contaminants which are ingested orally by consumers. Reported health concerns include intestinal translocation, inflammatory response, oxidative stress and cytotoxicity. Every digestive milieu in the gastrointestinal tract does have an influence on the properties of particles and can cause changes in their effect on biological systems. In this study, we subjected plastic particles of different materials (polylactic acid, polymethylmethacrylate, melamine formaldehyde) and sizes (micro- to nano-range) to a complex artificial digestion model consisting of three intestinal fluid simulants (saliva, gastric and intestinal juice). We monitored the impact of the digestion process on the particles by performing Dynamic Light Scattering, Scanning Electron Microscopy and Asymmetric Flow Field-Flow Fractionation. An *in vitro* model of the intestinal epithelial barrier was used to monitor cellular effects and translocation behavior of (un)digested particles. In conclusion, artificial digestion decreased cellular interaction and slightly increased transport of all particles across the intestinal barrier. The interaction with organic matter resulted in clear differences in the agglomeration behavior. Moreover, we provide evidence for polymer-, size- and surface-dependent cellular effects of the test particles.

1. Introduction

The production of plastic materials is rising since they have been invented. In 2019, the world production per year reached 460 million tons (Ritchie and Roser, 2022). Nowadays, products made of plastic can be found in every field of our lives and seem to be indispensable in many applications (Ritchie and Roser, 2022). The term plastics is the generic term for different polymer materials characterized through very diverse properties such as density, stability and degradability. Plastics can be categorized based on their physical properties relevant to manufacturing into thermoplastics, thermosets (durosets) and elastomers (Eyerer, 2010). Normally, a plastic product is designed for a special purpose by choosing a type of polymer and suitable additives; this is termed "primary plastics". It is estimated that in 2015 about 55 % of the global plastic waste was discarded, while about 25 % were incinerated and only 20 % were recycled (Ritchie and Roser, 2022). As a consequence, more than half of the plastic waste ends up in the environment, where it is continuously affected by different environmental factors, like UV radiation and mechanical stress (GESAMP, 2015; EFSA, 2016). These processes degrade the materials into smaller particles, reaching sizes in the micro- and nanometer range. The thereof resulting particles are named "secondary plastics". As ubiquitous environmental contaminants, micro- and nanoplastic particles can be transported through water and air, and end up in human food products like seafood, salt, beer or beverages (Toussaint et al., 2019).

The definition and categorization framework of micro- and nanoplastic particles is still subject of an unresolved debate that can lead to

* Corresponding author. German Federal Institute for Risk Assessment, Max-Dohrn Straße 8-10, 10589, Berlin, Germany.
E-mail addresses: maxi-birgit.paul@bfr.bund.de (M.B. Paul), linda.boehmert@bfr.bund.de (L. Böhmert), andreas.thuenemann@bam.de (A.F. Thünemann), kals@food.dtu.dk (K. Loeschner), lgiv@food.dtu.dk (L. Givelet), fahrenson@tu-berlin.de (C. Fahrenson), albert.braeuning@bfr.bund.de (A. Braeuning), holger.sieg@bfr.bund.de (H. Sieg).

https://doi.org/10.1016/j.fct.2023.114423
Received 11 September 2023; Received in revised form 19 December 2023; Accepted 21 December 2023
Available online 27 December 2023

Abbreviations

AF4	Asymmetric Flow Field-Flow Fractionation
DLS	Dynamic Light Scattering
DMEM	Dulbecco's modified eagle medium
EDTA	Ethylenediaminetetraacetic acid
EFSA	European Food Safety Authority
FCS	Fetal calf serum
FITC	Fluorescein-isothiocyanate
MALS	Multi-Angle Light Scattering
MF	Melamine formaldehyde resin
MTT	3-(4,5-dimethylthiazol-2-yl)-2,5- diphenyltetrazolium bromide
NAM	New approach methodologies
P/S	Penicillin/streptomycin
PBS	Phosphate-buffered saline
PDI	Polydispersity index
PE	Polyethylene
PLA	Polylactic acid
PMMA	Polymethylmethacrylate
PS	Polystyrene
SDS	Sodium dodecyl sulfate
SEM	Scanning Electron Microscopy
TEER	Transepithelial electrical resistance
UPW	Ultrapure water

misunderstandings. Hartmann et al. have suggested that the term "nanoplastic particles" refers to dimensions <1 μm (Hartmann et al., 2019). In contrast, we have decided to use the term "nano" as commonly used in the nanotoxicology field. Nanoparticles are well defined with an upper size limit of 100 nm by DIN CEN ISO/TS 80001-2 and also in European food and chemical regulation (Regulation No. 1169/2011 on the provision of food information to consumers). For microplastics, most studies use a lower size limit of 1 μm. Therefore, a gap in the definition of particles >100 nm but <1 μm arises. To fill this definition gap we here use the term "submicro". Especially the smaller submicro- and the nanoplastic particles are of high toxicological interest, but analytical methods are very limited (Caldwell et al., 2022). Various *in vitro* and *in vivo* studies have proven the capability of micro-, submicro- and nanoplastics to cross the gastrointestinal barrier after oral ingestion and even to enter the liver, as reviewed by for example by Khan and Jia et al. (Khan and Jia, 2023) or da Silva Brito et al. (da Silva Brito et al., 2022). Bioavailability of particles especially with a diameter <1.5 μm has also been concluded by the European Food Safety Authority EFSA (EFSA, 2016). When applying *in vitro* models of the gastrointestinal barrier, which are often based on the well-known cell line Caco-2, these cells are mostly incubated with pristine particles that did not undergo previous digestion through the oral cavity, stomach and intestine. Actually, there is first evidence that substances present in saliva, gastric or intestinal juices alter the properties and translocation of microplastics across the gastrointestinal barrier (Toto et al., 2022; Walczak et al., 2015; DeLoid et al., 2021). Thus, the aspect of digestive juices should be considered in an experimental setup related to the intestinal absorption of small plastic particles. However, investigating the effect of digestive fluids on particle behavior and properties can be challenging and is not always possible *in vivo*. Therefore, a combination of artificial digestion and *in vitro* models is reasonable and has already been used in previous studies, revealing changes in the protein corona (Walczak et al., 2015; Liu et al., 2020) or size (Liu et al., 2020; Stock et al., 2020) of plastic particles. Given that characteristics of particles might have a great influence on the uptake into intestinal cells, it should be expected that different polymer materials show changes in their uptake rate due to the influence of the organic matter of the digestive fluids.

On the basis of this, we have performed an artificial digestion and investigated the impact of saliva, gastric and intestinal juice on food-relevant micro-, submicro- and nanoplastic particles made of different polymer materials (polylactic acid (PLA), polymethylmethacrylate (PMMA) and melamine formaldehyde resin (MF)). We performed a set of suitable analytical measurements (Dynamic Light Scattering (DLS), Scanning Electron Microscopy (SEM), and Asymmetric Flow Field-Flow Fractionation (AF4) coupled to Multi Angle Laser Scattering (MALS) before, during and after incubation of the particles in complex and realistically simulated gastrointestinal fluids, in order to gain insight in the influence of the digestive process on the particles. After the digestion process, the particles were applied to differentiated Caco-2-based *in vitro* cell culture systems to study the uptake and transport across the intestinal barrier. Furthermore, cell viability and cellular impedance were measured to investigate the toxicological potential of the particles. Taken together, this study provides insight into the changes and behavior of different plastic particles during and after the gastrointestinal digestion process, and reveals details of their interaction with the intestinal barrier.

2. Methods/experimental

2.1. Chemicals and plastic particles

The chemicals used for this study were purchased from Merck KgaA (Darmstadt, Germany), Carl Roth GmbH & Co. KG (Karlsruhe, Germany), or Sigma-Aldrich Chemie GmbH (Taufkirchen, Germany) if not otherwise indicated.

All plastic particles were ordered as aqueous dispersion and with fluorescence labels. Polylactic acid polydisperse microparticles with a nominal diameter of 2000 nm (**PLA2000**, stock concentration: 2.40 x 10^9 particles/mL) and submicroparticles of the same material with a mean diameter of 250 nm (**PLA250**, stock concentration: 1.2 x 10^{12} particles/mL) were purchased from Micromod particle technology GmbH (Rostock, Germany, PLA-greenF, prod. no: 51–00-252 and 51–00-203). These particles have a fluorescence label of Ex/Em 502/527 nm. Submicrometer particles made of melamine formaldehyde resin with a mean diameter of 366 nm were ordered from Microparticles GmbH (Berlin, Germany, charge: MF-FluoOrange-S886–1) and have a fluorescence label of Ex/Em 560/584 nm (**MF366**, stock concentration: 3.07 x 10^{10} particles/mL). Nanoplastic particles made from polymethylmethacrylate (mean diameter: 25 nm) were purchased from Creative Diagnostics (New York, USA, DiagPoly™ Plain Fluorescent PMMA nanoparticles, cat. no.: DNG-P010). These particles have a fluorescence label of Ex/Em 475/510 nm (**PMMA25**, stock concentration: 1.20 x 10^{15} particles/mL). The particles have been characterized in an earlier publication by our group (Paul et al., 2022). Briefly, diameters given by the manufacturer were confirmed by SEM, DLS and AF4. PLA2000 and PLA250 had hydrophobic properties, while MF366 and PMMA25 had hydrophilic characteristics. The particles have been checked for fluorescence leakage within the hydrophobicity measurements and a loss of fluorescence signal was excluded. Due to the widely varying sizes of the particles, we chose to use the unit particle surface per mL, so that the concentrations used for the incubation are comparable.

2.2. Artificial in vitro digestion

The artificial *in vitro* digestion protocol is originally based on DIN 19738 for "Soil quality - Bioaccessibility of organic and inorganic pollutants from contaminated soil material", which was modified by

Oomen et al. and Versantvoort et al. in order to determine the bioaccessibility of orally ingested compounds like heavy metals or other contaminants (Versantvoort et al., 2005; Oomen et al., 2003). Based on this work, a number of groups adopted the *in vitro* digestion for the investigation of nanoparticles, like silica nanoparticles (Peters et al., 2012; Walczak et al., 2012), polystyrene (PS) nanoparticles (Stock et al., 2020; Walczak et al., 2015), silver nanoparticles (Lichtenstein et al., 2015; Böhmert et al., 2014; Kästner et al., 2017, 2018; Abdelkhaliq et al., 2020), aluminum-containing nanoparticles (Sieg et al., 2017, 2020), and zinc oxide nanoparticles (Voss et al., 2019, 2021). The experimental design comprises three complex digestive fluids to simulate saliva, gastric juice and intestinal juice as realistic as possible. Their components and pH values are given in Fig. 1. The experiment was conducted at 37 °C in a water bath under constant stirring. The stock dispersions of the particles PLA2000, PLA250, MF366 and PMMA25 were diluted each in artificial saliva as shown in Fig. 1 to a final saliva volume of 14 mL. As a control, 14 mL of saliva without particles was also incubated. The artificial saliva samples including one particle species each were incubated for 5 min. In the next step, 5 mL of the saliva were abstracted for further analysis. The remaining 9 mL were filled up with 21 mL of artificial gastric juice. The pH was adjusted to 2 by using hydrochloric acid. After incubating the mixture for another 2 h, another sample of 5 mL volume was removed for further analysis. Subsequently, 25 mL of the artificial intestinal juice was added to the remaining 25 mL of the mixture. The pH was adjusted to a value of 7.5 by using sodium bicarbonate powder. The assortment was incubated for 2 h and used for further analysis. The activity of the digestive enzymes was checked during the experiment by measuring enzymatic cleavage products via photometric analysis as a control. For saliva, amylase activity was checked by amylopectin azure (Phadebas® Amylase test, Phadebas AB, 291 96 Kristianstad, Sweden). For gastric juice, the albumin/-bromophenol blue complex was used to verify pepsin activity (see (Gray

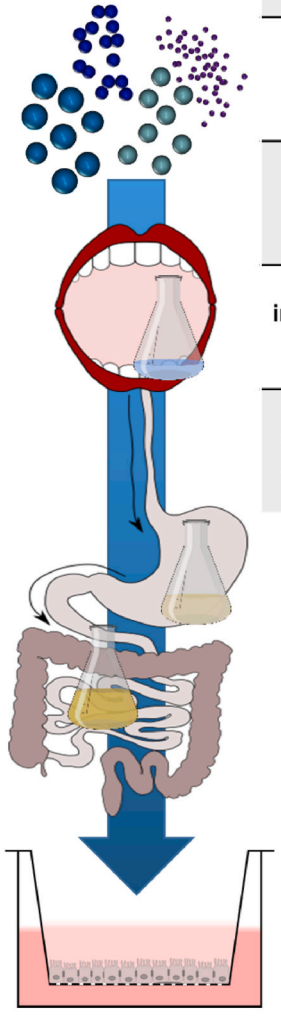

		PLA2000	PLA250	MF366	PMMA25
stock concentration [μm^2 particle surface/mL]		$3.00x10^{10}$	$2.40x10^{11}$	$2.74x10^{11}$	$2.02x10^{12}$
saliva	dilution factor	4.11	30.30	3.60	4.50
	concentration [μm^2 particle surface/mL]	$6.67x10^{9}$	$6.67x10^{10}$		
gastric juice	dilution factor	3.33			
	concentration [μm^2 particle surface/mL]	$2.00x10^{9}$	$2.00x10^{10}$		
intestinal juice	dilution factor	2.00			
	concentration [μm^2 particle surface/mL]	$1.00x10^{9}$	$1.00x10^{10}$		
cellular assays	dilution factor	20.00			
	concentration [μm^2 particle surface/mL]	$5.00x10^{7}$	$5.00x10^{8}$		

Composition of digestion fluids

saliva pH 6.4	**gastric juice** pH 2.0	**intestinal juice** pH 7.5
1.667 mg/mL NaCl	4.143 mg/mL NaCl	0.3 mg/mL NaCl
0.5 mg/mL NaSCN	1.0 mg/mL KCl	0.5 mg/mL NaSCN
1.833 mg/mL Na_2SO_4	0.386 mg/mL KH_2PO_4	0.5 mg/mL $NaHCO_3$
0.5 mg/mL $NaHCO_3$	4.286 mg/mL Mucin	0.3 mg/mL Trypsin
1.5 mg/mL KCl	1.429 mg/mL Pepsin	0.3 mg/mL Urea
2.0 mg/mL KH_2PO_4	HCl for titration	0.5 mg/mL $CaCl_2 \cdot H_2O$
0.5 mg/mL $CaCl_2 \cdot H2O$		0.2 mg/mL $MgCl_2 \cdot 6\ H_2O$
0.33 mg/mL Ureate		9.0 mg/mL Pancreatin
0.033 mg/mL Urea		9.0 mg/mL Bile extract
0.833 mg/mL α-Amylase		$NaHCO_3$ (s) for titration
2.5 mg/mL Mucin		

Fig. 1. Overview of the artificial digestion process and following incubation on differentiated Caco-2 cells grown on Transwell™ membranes. The upper table gives an overview of the concentrations of the applied particles in the respective digestive juices and subsequent cellular assays. The lower table depicts the composition of saliva, gastric and intestinal juice.

and Billings, 1983)); pepsin was from AppliChem GmbH (Darmstadt, Germany). For intestinal juice, the activities of lipase and trypsin were measured by using 4-methylumbelliferyl oleate and azocasein, respectively (see (Bitou et al., 1999)); trypsin 1:250 from porcine pancreas was from AppliChem GmbH (Darmstadt, Germany).

2.3. Analytical methods

SEM, AF4-MALS and DLS were performed as analytical methods to characterize the (un)digested samples. For some methods, a reduction of organic matter from the artificial digestion process was required. To degrade the organic matter that surrounds the particles after *in vitro* digestion, an aliquot of each sample was taken and treated with a 15 % hydrogen peroxide (H_2O_2) solution for 16 h at room temperature, adopted from a protocol by Frias et al. (2018), for microplastics in sediments (Frias et al., 2018). Additionally, enzymatic sample preparation was chosen as another method to degrade the organic matter.

2.3.1. SEM

Changes of size and morphology of the particles in the digestive environment were determined by scanning electron microscopy (SEM) using a Zeiss DSM 982 Gemini (Carl Zeiss AG, Oberkochen, Germany; updated by point electronic GmbH, Halle (Saale), Germany) and a Zeiss GeminiSEM500 NanoVP in LowVacumMode (Carl Zeiss AG, Oberkochen, Germany). To analyze the samples, one drop of the (un)digested particles, undiluted or diluted in cell culture medium, was placed on a silica wafer and air-dried. The measurement was conducted with an acceleration voltage ranging from 3 to 9 kV on the basis of a previous study using the same micro-, submicro- and nanoplastic particles (Paul et al., 2022).

2.3.2. AF4-MALS

AF4-MALS was applied to determine the changes of the particle size distribution based on root mean square diameters (d_{rms}) of PLA250 and MF366 samples. The AF4 system consisted of an Agilent 1200 series autosampler (G1329A), a high-performance liquid chromatography pump (G1311A) (Agilent Technologies, Santa Clara, CA, USA), an Eclipse 3 AF4 flow control module, and a short channel-type AF4 separation channel with a 350 μm spacer (Wyatt Technology Europe GmbH, Dernbach, Germany). The carrier liquid was ultrapure water (UPW) containing the alkaline detergent mix Fisherbrand FL-70 (Fisher Scientific, Pittsburgh, MA, USA) at a concentration of 0.025 % (v/v) as in previous work (Paul et al., 2022). As membrane material regenerated cellulose with a 10 kDa cut-off was used. Following separation by AF4, a DAWN HELEOS TM (Wyatt Technology Europe GmbH, Dernbach, Germany) MALS detector with 17 observation angles operated with a linear polarized laser light at 658 nm was used to record the light scattering signal. The data collection interval was set to 2 s. Light scattering data was processed using the ASTRA V software (version 5.3.4.20, Wyatt Technology Corporation, Santa Barbara, CA, USA). The MALS detector at angle 90° was used for detection of the particles. The d_{rms} was determined using a 3rd order Debye model. Before analysis, the samples were diluted in carrier liquid aiming at similar injected particle masses for each sample (1 μg for PLA250, 3 μg for MF366). Samples were either diluted as received or after enzymatic digestion. Enzymatic digestion was based on a protocol used by Correia and Loeschner and used to reduce the influence of organic components from the *in vitro* digestion on the separation (Correia and Loeschner, 2018). The enzyme solution was prepared by diluting 3 mg/mL of Proteinase K in digestion buffer containing 50 mM ammonium bicarbonate (with 99 % purity), 5 mg/mL sodium dodecyl sulfate (SDS, ReagentPlus with ≥98.5 % purity), and 0.2 mg/mL sodium azide (with ≥98 % purity). A volume of 2 mL of enzyme solution was added to 0.1 mL of sample, which was then placed in a water bath at 37 °C (HetoHMT 200 RS thermostat) and magnetically stirred with the use of Telesystem HP15 magnetic stirrer (Holm & Halby, Allerød, Denmark) overnight (17 h). At the end of the enzymatic treatment, the completely digested samples were placed on ice to slow down the enzymatic digestion process, and appropriately diluted with UPW prior to AF4 analysis. The separation program is depicted in Table S1. The detection flow was 1 mL/min, the focus flow 0.5 mL/min, the injection flow 0.1 mL/min. The injection volume was 50 μL per sample.

2.3.3. DLS

The particle size distribution based on hydrodynamic diameters was quantified, for the samples analyzed by AF4-MALS, by use of a Zetasizer Nano ZS (Malvern Panalytical GmbH, Kassel, Germany). For measurements, the undigested or digested particles in either saliva, gastric juice or intestinal juice were diluted approximately 1:1000 in UPW and subsequently measured. The measurements were carried out using disposable folded capillary zeta cells (DTS1070, Malvern Instruments, UK). The angle of detection was 173° and the temperature was 25 °C. The measurement position and the laser power (attenuator index) were determined automatically by the instrument. Typical values for all samples were a measurement position of 5.5 mm and an attenuator index of 8–11. The DLS characteristics of the measured sample, given as Z-average (intensity-weighted harmonic mean diameter) and polydispersity index (PDI) were determined by averaging three replicate measurements.

Further, DLS measurements of the digested particles diluted in cell culture medium were performed with a Litesizer 500 (Anton Paar, Graz, Austria) at a scattering angle of $2\theta = 90$ ° and a temperature of 23 °C. The laser wavelength was $\lambda = 658$ nm, the refractive index $n = 1.33$ and the scattering vector $q = 0.0180\ \mathrm{nm}^{-1}$ ($q = 4\pi/\lambda \sin(\theta/2)$). Single measurements with a duration of 10 s were repeated 60 times and averaged. Samples were taken after the complete digestion process and were diluted in a ratio of 1–99 (v/v) with complete cell culture medium and subsequently measured.

Samples taken after the complete digestion procedure (i.e., particles in intestinal juice and control without particles) were further analyzed *in vitro*. Therefore, the well-known colon carcinoma cell line Caco-2 was used, that differentiates spontaneously into intestinal-like cells after reaching confluence (Lea, 2015). The Caco-2 cells (ECACC: 86010202) were obtained from the European Collection of Authenticated Cell Cultures (Salisbury, UK). Cultivation of the cells was realized at 37 °C and 5 % CO_2. The cell culture medium for Caco-2 cells consisted of Dulbecco's Modified Eagle Medium (DMEM; Pan-Biotech GmbH, Aidenbach, Germany) supplemented with 10 % (v/v) fetal calf serum superior (FCS superior) and 10^5 Units/L penicillin and 100 μg/mL streptomycin (P/S; Capricorn Scientific GmbH, Ebsdorfergrund, Germany). The cells were cultivated as described before (Stock et al., 2021; Paul et al., 2022, 2023). In short, Caco-2 cells were maintained between 80 and 90 % confluence and passaged every 2–3 days by washing the cells with phosphate-buffered saline (PBS) and adding 0.05 % trypsin-ethylenediaminetetraacetic acid (trypsin-EDTA) at 37 °C for 5 min.

2.3.4. Cell viability measurements

The potential cytotoxic impact of the digested particles and/or the digestive juice was investigated by the 3-(4,5-dimethylthiazol-2-yl)-2,5-diphenyltetrazolium bromide (MTT) assay. For this experiment, 5000 Caco-2 cells/well were seeded in a 96-well plate and differentiated for three weeks. For incubation, the digested particles and the digestive juice were diluted either 1:10, 1:20, or 1:40 (30 + 270 μL, 15 + 285 μL or 7.5 + 292.5 μL of digestive mixture and medium, respectively) in phenol red-free cell culture medium. As positive control, 0.01 % Triton X-100 was applied. A volume of 100 μL of each sample was pipetted on the cells and incubated for 24 h at 37 °C. Afterwards, the incubation medium was removed and replaced by 100 μL/well of phenol red-free cell culture medium. The MTT reagent was diluted in PBS to a final concentration of 5 mg/mL, a volume of 10 μL/well was added to the cells and incubated for 1 h at 37 °C. The incubation medium was aspirated and 130 μL/well

desorption solution (0.7 % (w/v) SDS in isopropanol) were added. The plates were shaken for 30 min under light exclusion at room temperature. The absorption was measured in a Tecan plate reader (Plate Reader Infinite® M200Pro; Tecan Group Ltd., Männedorf, Switzerland) at 570 nm and at 630 nm background absorption. For evaluation, the obtained data were subtracted by background signals without cells and related to the controls (either cell culture medium or digestive juice). The control value was set to 100 %.

In addition, the xCELLigence® Real Time Cell Analysis (Agilent Technologies Germany GmbH & Co. KG, Waldbronn, Germany) was applied to investigate potential effects of the digested particles and the digestive fluid during an incubation time of 3 days. Caco-2 cells were seeded in 96-well microplates (5000 cells/well), which were coated with gold microelectrodes to deliver a measured value to the device. After three weeks of differentiation, the cells were incubated with 150 µL of the digested particles or digestive juices (1:10, 1:20, 1:40 dilution). Cell culture medium served as negative control and 50 µg/mL zinc oxide as positive control.

2.3.5. Cellular uptake and transport

For uptake and transport experiments, the Caco-2 barrier model based on a 12-well Transwell™ plate (Corning Incorporated, New York, USA) was used. This plate has inserts in each well, which consist of a polycarbonate membrane with 1.12 cm^2 growth area and 3 µm pores. Hence, the well is separated into an apical and a basolateral compartment. For differentiation of Caco-2, 50,000 cells per well were seeded on the membrane of the inserts in Caco-2 culture medium and let differentiate for three weeks. The cell culture medium was refreshed every 2–3 days in both compartments. After differentiation, the integrity of the Caco-2 monolayer was verified via transepithelial electrical resistance (TEER, EVOM2 electrode (World Precision Instruments, Sarasota, Florida, USA)) measurements and leakage of 10 kDa fluorescein isothiocyanate (FITC)-dextran. Permeability values $> 700\ \Omega*cm^2$ for TEER and P_{app} values $< 10^7$ cm/s calculated from FITC-dextran transport confirmed an intact monolayer.

The differentiated cells were further incubated for 24 h with digested particles diluted 1:20 in cell culture medium (concentrations see Fig. 1), or with undigested particles diluted to the same end concentration as used for the digested samples. The digestive juice without particles (dilution 1:20 in medium) and pure cell culture medium served as additional controls. To do so, the cell culture medium was replaced by 500 µL of the diluted sample in the apical compartment and 500 µL cell culture medium in the basolateral compartment. After 24 h, supernatants of the apical and basolateral compartment, as well as a washing fraction (2 x 250 µL PBS), were collected. The fluorescence signal of each fraction was measured and a calibration curve in the respective medium (cell culture medium or PBS) of each particle type was produced, from which the particle concentration was finally calculated. For quantification, the Tecan plate reader was used. The Transwell™ membrane containing the Caco-2 cells was incubated for 30 min at 37 °C in a fixation solution of 3.7 % formaldehyde in PBS. The fixed membranes were washed 3 times with PBS and analyzed for their fluorescence signal in a Tecan plate reader. To be able to quantify the intensity, the addition method was used. Therefore, a known amount of the particles used for incubation was added five times and the signal measured after each time. From this, we calculated a standard curve for each particle.

2.3.6. Staining and microscopy

The membranes were then prepared for microscopic investigation. Therefore, the membranes were washed with PBS and cells were permeabilized in a 0.2 % Triton X-100 solution in PBS for 20 min at room temperature. Finally, the membrane was washed again three times and stained for 30 min under exclusion of light with 2 drops/mL ActinGreen 488 ReadyProbes® Reagent (for MF366 and controls) or 2 drops/mL ActinRed 555 ReadyProbes® Reagent (for PLA and PMMA; Life technologies, New York, USA) as described by the manufacturer. For microscopy, the membranes were cut off the insert and fixed on a microscope slide with Kaiser's glycerin gelatin (Carl Roth GmbH + Co. KG, Karlsruhe, Germany). The slides were dried at 4 °C and further analyzed using a laser scanning confocal microscope LSM 700 (Carl Zeiss AG, Oberkochen, Germany). For investigation, the XYZ acquisition mode, 63x objective and contrast adjustment were used. To get an overview of the particle distribution, 4 to 5 randomly selected parts of the membrane were investigated.

Furthermore, fluorescence microscopy was applied to investigate the particle distribution across the Caco-2 cell monolayer. For sample preparation, the digested particles and their control were additionally incubated on differentiated Caco-2 cells seeded in 96-well plates (5000 cells/well, same particle concentration). After 24 h of incubation, the wells were washed with PBS and analyzed with the inverse microscope axio observer d1 (Carl Zeiss, Oberkochen, Germany) using the bright-field, EGFP (Ex/Em 488/509), or Cy3 (Ex/Em 548/561 nm) filters, depending on the fluorescence label of the particles. Images were recorded at 50x magnification.

3. Results

3.1. In vitro cellular assays with (un)digested plastic particles

To assess the toxicological impact of the digested particles on intestinal cells, differentiated Caco-2 cells were incubated with different dilutions (1:40, 1:20, 1:10) of each digested particle sample in cell culture medium, as well as with the intestinal fluid without particles at the same dilutions. Cell viability and cellular impedance were investigated using MTT and xCELLigence® measurements (Fig. 2, Fig. 3). The artificial intestinal fluid showed non-toxic properties at the 1:40 and 1:20 dilutions, whereas a dilution of 1:10 resulted in a slight decrease of viability of about 20 %. For all digested particle species, viability values of the 1:40 and 1:20 dilutions varied around 100 % as well, while a 1:10 dilution again reduced viability values to 60–80 % (Fig. 2 A). The bottom diagram (Fig. 2 A) shows the cell viability, normalized to the effects of the digestion controls in each dilution. Here it becomes obvious that only Caco-2 cells incubated with digested MF366 show a slight dose-dependent viability decrease, which exceeds the effects of the digestion controls. The other plastic materials induced no further effects beyond the toxicity caused by the digestion controls. In Fig. 2 B, representative fluorescence microscopic images of differentiated Caco-2 cells incubated with the 1:20 dilution of digested and undigested particles are shown. The images of the single channels can be found in Fig. S1. The cells showed no morphological changes following incubation with the digested particles or the intestinal juice, as compared to incubation with the undigested particles. All particle species were taken up by the cells or adhered to their surface. For PMMA25, only a very low particle-cell interaction was observed. The most pronounced particle-cell interaction was identified for the submicrometer particles MF366 and PLA250. The agglomeration of particles differed between the materials, as PLA250 was allocated all over the cell surface and MF366 agglomerated in parts of the cells, independent of the digestion process.

Fig. 3 shows the changes in cellular impedance of differentiated Caco-2 cells after incubation with the abovementioned diluted digested particles over a time period of 72 h, which corresponds to the lifespan of *in vivo* intestinal epithelial cells. In the upper diagram, the effects of diluted simulated intestinal fluid without plastic particles are depicted. During the observed time span, dilutions of 1:40 and 1:20 showed no changes in cell impedance, while a dilution of 1:10 induced changes in cell impedance, expressed by slightly increased impedance values. The other diagrams show the effects of accordingly diluted digested plastic particles, which produced similar results. Only when diluted 1:10 in cell culture medium, changes in cell indices were visible, as for the control conditions. Overall, the effects were very mild, not indicating any toxic effects on intestinal barrier integrity.

In Fig. 4, the cellular interaction and transport of (un)digested micro-

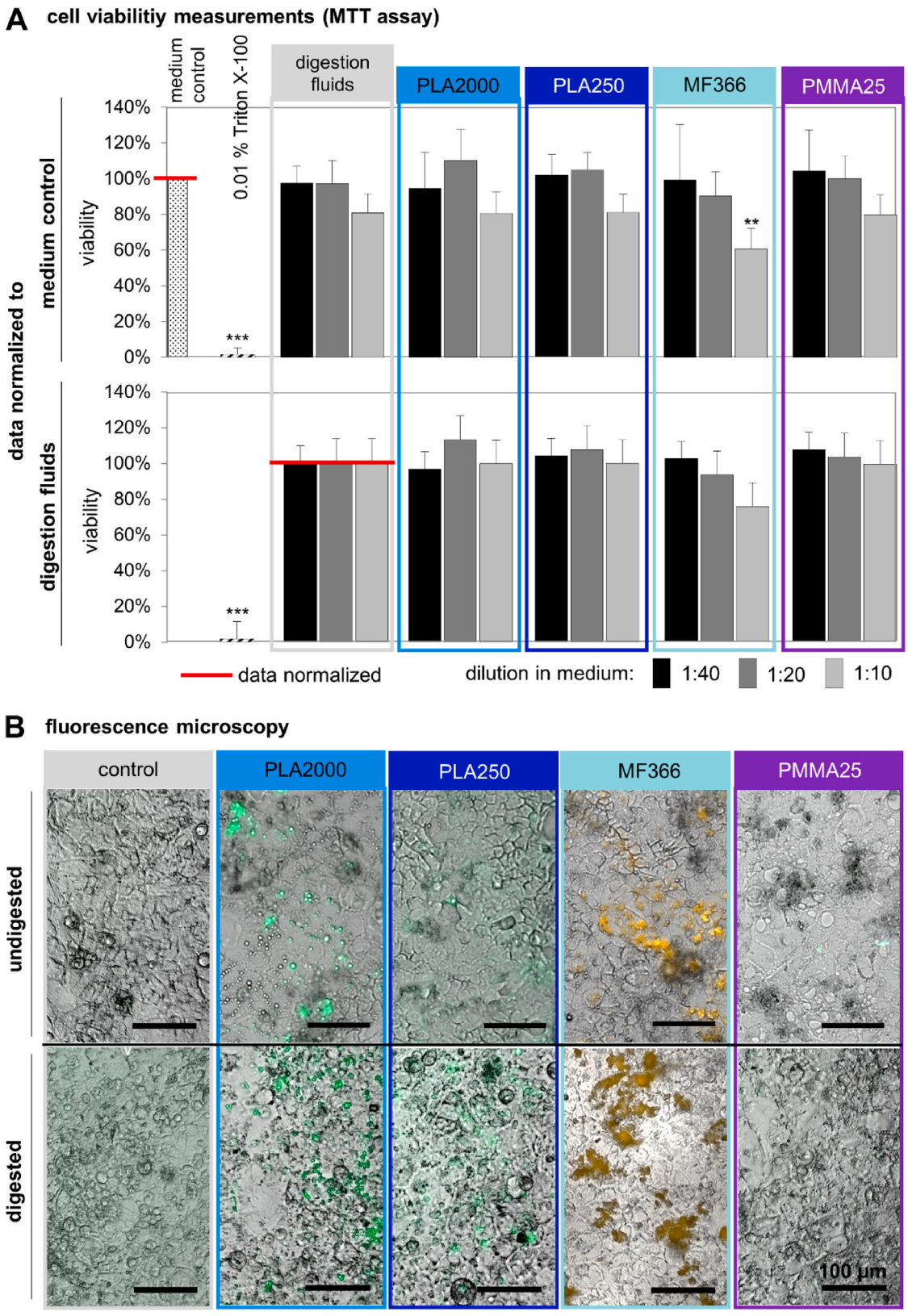

Fig. 2. Toxicological impact of digested particles on differentiated Caco-2 cells, as measured by the MTT assay (**A**) and by fluorescence microscopy (**B**). **A**: Results of the MTT assay after 24 h incubation with digested particles or intestinal juice at dilutions of 1:10, 1:20 and 1:40. 0.01 % Triton X-100 served as positive control. The results were either normalized to medium control (**upper diagram**), or to the respective dilution of intestinal juice diluted in medium (**lower diagram**). Data are presented as means with SD, n = 3. Significance was calculated with one-way ANOVA followed by Dunnett's test (*p ≤ 0.05; **p ≤ 0.001; ***p < 0.001). **B**: Representative fluorescence microscopy images of either undigested (upper images) or digested (lower images) particles and controls (medium or intestinal juice) incubated for 24 h on differentiated Caco-2 cells (1:20 dilution). Particles are shown in green or orange. (For interpretation of the references to colour in this figure legend, the reader is referred to the Web version of this article.)

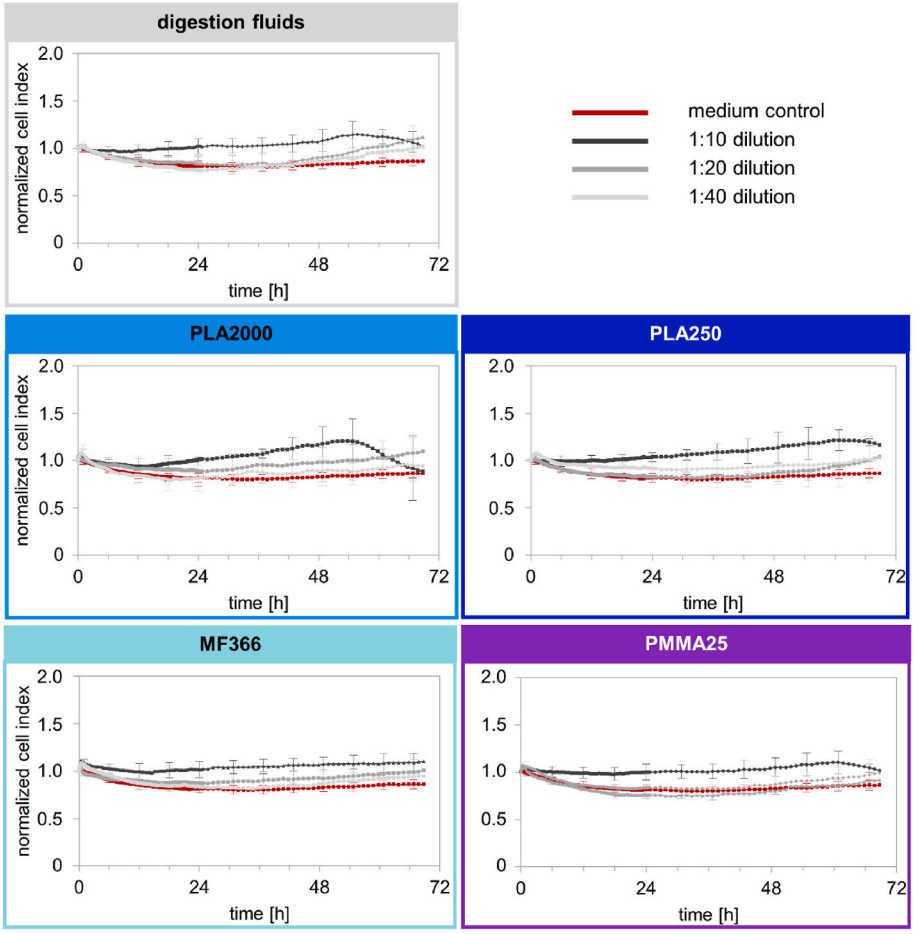

Fig. 3. Changes in cellular impedance of differentiated Caco-2 cells incubated with different dilutions (1:10, 1:20, 1:40) of digested particles or the intestinal juice, as measured for 72 h with xCELLigence® Real Time Cell Analysis. Cell culture medium served as negative control. Data are presented as means ± SD, n = 3.

, submicro- and nanoplastic particles through the intestinal barrier are shown. The particles were incubated for 24 h on differentiated Caco-2 cells, grown on Transwell™ membranes as presented in Fig. 4 A. The tightness of the monolayer was checked via TEER measurements and FITC-dextran leakage, and the results (Fig. S2) proved an intact monolayer. The quantification of particles present in the membrane fraction (in and on the Caco-2 cells, Fig. 4 B) showed differences between undigested and digested plastic particles: For pristine particles, the cellular interaction of submicrometer PLA250 and MF366 particles was around 30 % of the applied dose. For the PLA2000 polydisperse microplastic, an interaction of 21 % was quantified in the membrane fraction. In contrast to that, the presence of PMMA25 nanoplastics was almost undetectable. Interestingly, the cellular interaction with the digested particles decreased distinctly, as compared to undigested particles. For all measured samples, a maximum value of 8 % was calculated. In Fig. 4 C, the transport of (un)digested plastic particles across the intestinal barrier was quantified. In contrast to the pristine particles, where the transport ranged from 2 % to 11 %, the transport of digested particles was slightly higher and differed between materials and particle sizes. Only for PLA2000, comparable transport rates of digested and undigested particles were observed. The highest transport of 31 % was quantified for PMMA25, followed by both PLA particles with 15 % transport. The lowest transport was measured for digested MF366. Which was only slightly higher than for the undigested MF366 particles.

To verify the data presented in Fig. 4, the cell membrane fractions, as well as the basolateral fractions, were analyzed with confocal and fluorescence microscopy (Fig. 5). Confocal microscopy was used to compare the presence of particles inside the Caco-2 cells between undigested (Fig. 5 B, left column) and digested (Fig. 5 B, right column) particles. The cell monolayer was not impaired under any of the tested conditions. All particles (PLA2000, PLA250 and MF366) except PMMA25 nanoparticles were present inside the cells independent of the digestion, but at smaller amounts. Especially for PLA250, the uptake of digested particles decreased, as compared to pristine particles. In Fig. 5 C, representative images of the PLA2000, PLA250, MF366 and PMMA25 particles detected in the basolateral fraction of the Transwell™ experiment are shown. Specifically, these particles were transported through the intestinal barrier.

3.2. *Analytical studies of plastic particles during the artificial digestion*

This artificial digestion process of PLA2000, PLA250, MF366 and PMM25 was monitored by several analytical methods, including Scanning Electron Microscopy (SEM), Asymmetric Flow Field-Flow Fractionation coupled to MALS (AF4-MALS) and Dynamic Light Scattering (DLS). Detailed results are presented in the following text.

The analysis of polydisperse PLA2000 microparticles, the submicrometer particles PLA250 and MF366, as well as PMMA25 nanoparticles with SEM is presented in Fig. 6. Pristine particles (undigested stock dispersions) were detected easily, as there was no disturbing organic matter covering the particles. For the particle dispersions in cell culture medium, in the digestive fluids, and in the combination of digestive fluids and cell culture medium, the visualization of particles by SEM was disturbed by the dried surrounding fluids. Particles were recognized only for MF366 in saliva and gastric juice. A mild treatment of the samples with hydrogen peroxide, as used in a previous study

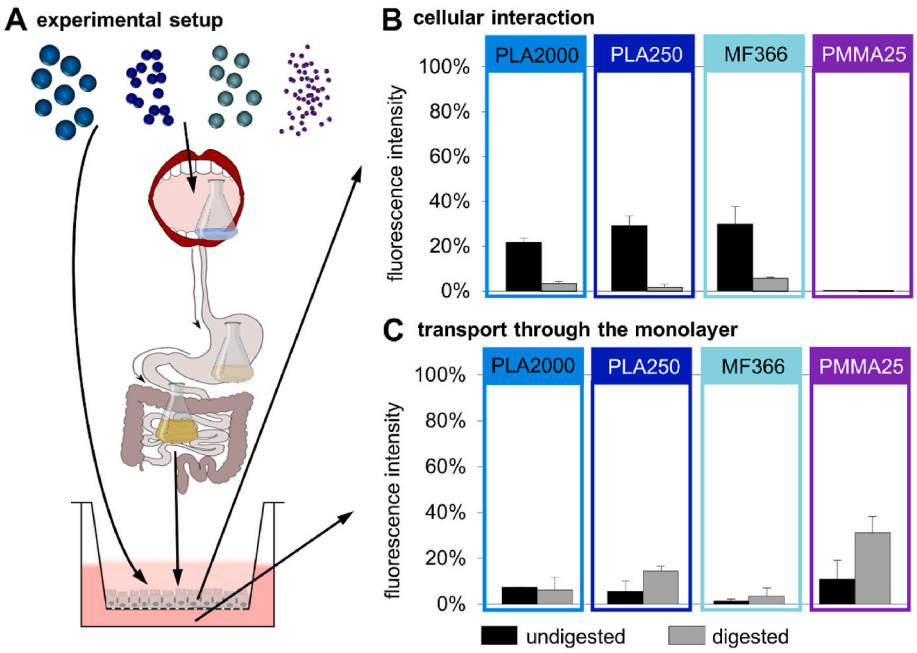

Fig. 4. Investigation on cellular interaction and transport of (un)digested micro-, submicro- and nanoplastic particles after 24 h incubation on differentiated Caco-2 cells. **A**: Schematic overview of the experimental setup. PLA2000, PLA250, MF366 and PMMA25 were incubated in artificial digestion juices (saliva, gastric juice, intestinal juice) to simulate human digestion. The digested particles were incubated on Caco-2 cells, differentiated on Transwell™ membranes, for 24 h (1:20 dilution). Undigested particles served as controls. **B**: Quantification of cellular interaction of particles with the Caco-2 cells (quantification of the fluorescence signal of the particles in and on the cells). Data are presented as means with SD, n = 3. **C**: Quantification of the transport of particles through the Caco-2 monolayer (quantification of the fluorescence signal of particles in the basolateral compartment). Data are presented as means with SD, n = 3.

(Stock et al., 2020), was not efficient enough in removing organic material (data not shown).

The SEM images revealed that the particles are surrounded by organic matter, and, moreover, the translocation studies showed differences between digested and undigested particles especially regarding cellular interaction. To further elucidate these observations, we applied AF4-MALS and DLS to obtain more detailed information on the behavior of the particles during digestion. We focused on the submicrometer particles PLA250 and MF366, because of their comparability due to similar diameters. Additionally, we have already shown in previous studies that these particles exhibit different surface properties, presumably leading to divergent uptake patterns (Paul et al., 2022),

The results of the AF4-MALS analysis are given in Fig. 7 A/B. The separation of the samples after additional enzymatic digestion is presented in the lower row ("with sample preparation"). AF4 separation of PLA250 (left column) showed that the elution profiles and the determined diameters of the undigested particles and the particles after contact with saliva were very similar (d_{rms} from ~100 to 260 nm). The sizes increased in the gastric stage (d_{rms} from ~220 to 280 nm across the elution peak) and early elution of large particles probably due to steric elution was observed. Enzymatic digestion did not remove these large particles, confirming that these were large agglomerates of the plastic particles rather than organic matter. The high void peak (time 0) of the enzymatically digested sample was caused by the enzyme itself. A low and noisy light scattering signal was obtained for the intestinal stage and the contribution of the components eluting in the void peak (retention time 0) increased. The constant d_{rms} values across the peak indicated non-ideal elution. Enzymatic digestion improved the separation and similar sizes as in the gastric stage could be obtained (d_{rms} from ~220 to 290 nm across the elution peak, again overlapped with early eluting agglomerates), indicating that organic matter had interfered with the separation.

MF366 particles in saliva eluted in a much broader peak than the undigested particles. The light scattering signal was noisy despite its relatively high intensity. Despite the peak broadening the sizes obtained by MALS were similar for undigested particles and particles in saliva (d_{rms} from ~250 to 280 nm). A narrower peak was observed after enzymatic digestion. For the gastric stage, the peak showed an unusual shape and early elution. The separation was strongly improved by enzymatic digestion, and similar peak shape and particle sizes compared to the mouth stage (d_{rms} from ~250 to 280 nm) were determined. Analysis of the particles from the intestinal stage without enzymatic digestion was not attempted due to the poor separation at the gastric stage. After enzymatic digestion, similar results for the mouth and stomach stage were obtained. Overall, no changes of the particle sizes for MF366 during the *in vitro* digestion, but an increase in particle sizes in the gastric and intestinal fluid for PLA250 were detected.

These AF4 separations were accompanied by DLS measurements before separation. The results for both submicroparticles are given in Fig. 7 C/D. In the first step of saliva, PLA250 had a similar size as the pristine particles but a higher PDI. The z-average and PDI increased in gastric juice and further in intestinal juice. The influence of the light scattering of the components in gastric/intestinal juice on the determined sizes cannot be neglected as similar derived count rates were observed in PLA250 samples and controls. Sizes were in general similar to the size ranges determined by AF-MALS, also considering that root-mean-square diameters are always smaller than hydrodynamic diameters. For MF366 the z-average and PDI increased already significantly in saliva, as compared to the pristine particles. No significant further increase in size was observed in gastric or intestinal juice. The obtained sizes were four- to five-fold larger than the ones determined by AF4-ICP-MS. This is in agreement with the observed strong influence of the digestion fluids on the separation behavior, which could be drastically reduced by enzymatic digestion.

3.3. DLS evaluation of digested plastic particles in cell culture medium

After passing through the digestion process, the particles are in the intestinal fluid and were diluted in cell culture medium (DMEM supplemented with 10 % FCS and 1 % P/S) for cellular assays. To further

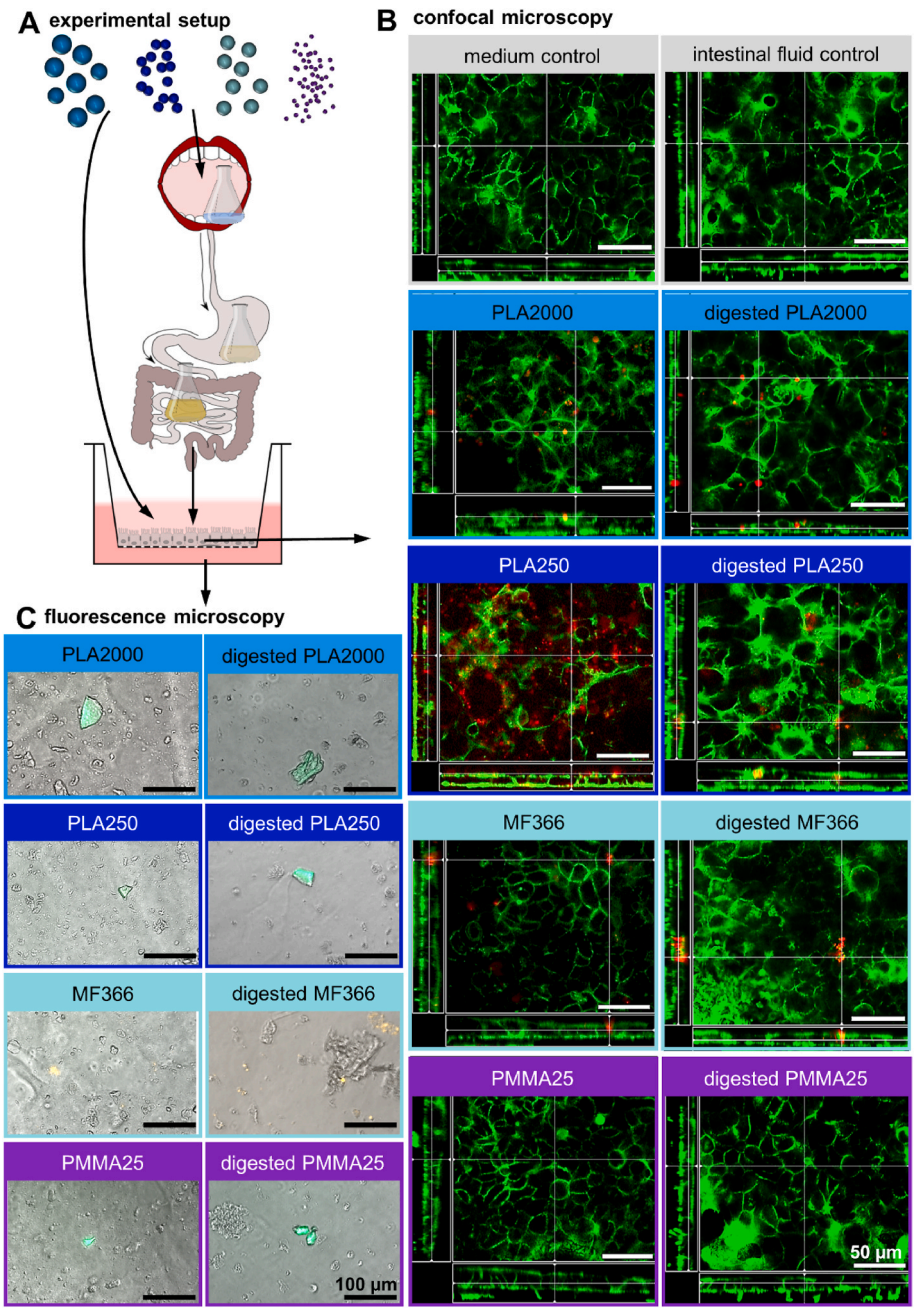

Fig. 5. Microscopic images of cellular interaction and transport of (un)digested micro-, submicro- and nanoplastic particles after 24 h incubation on differentiated Caco-2 cells. **A**: Schematic overview of the experimental setup. PLA2000, PLA250, MF366 and PMMA25 were incubated in artificial digestion juices (saliva, gastric juice, intestinal juice) to simulate human digestion. The digested particles were incubated on Caco-2 cells, differentiated on Transwell™ membranes, for 24 h (1:20 dilution). **B**: Representative confocal images of undigested (left) and digested (right) particles present within the intestinal monolayer. Caco-2 cells are shown in green and particles in red. **C**: Representative fluorescence images of the undigested (left) and digested (right) particles present in the basolateral compartment. (For interpretation of the references to colour in this figure legend, the reader is referred to the Web version of this article.)

analyze potential changes of the digested particles if diluted in cell culture medium, DLS has been performed. However, the applied dilution to be tested results in a medium that is quite complex for DLS measurement. Therefore, the question arises how to evaluate the DLS data. In the literature, from an analytical point of view, the best comparable system is polymeric nanoparticles and their aggregation in blood serum as reported by Rausch et al. (2010). Instead of blood serum, cell culture medium is used as particle medium here. With this approach, the evaluation is then as follows. According to Rausch et al., the electric field time autocorrelation function may be represented by

$$g_1(\tau) = f_s g_{1,s}(\tau) + g_{1,np}(\tau) + g_{1,agg}(\tau)$$

With f_s as a weighting factor ranging between 0 and 1. $g_{1,s}(\tau)$ is the electric field time autocorrelation functions of pure cell culture medium which can be fitted by the sum of three exponentials as

$$g_{1,s}(\tau) = a_{1,s}e^{-\tau/\tau_{1,s}} + a_{2,s}e^{-\tau/\tau_{2,s}} + a_{3,s}e^{-\tau/\tau_{3,s}}$$

Later, when fitting the $g_1(\tau)$ data of the digested particles diluted in cell culture medium, $g_{1,s}(\tau)$ is held constant and only the weighting factor f_s accounts for the contribution of cell culture medium for fitting $g_1(\tau)$. Non-aggregated particles are represented by

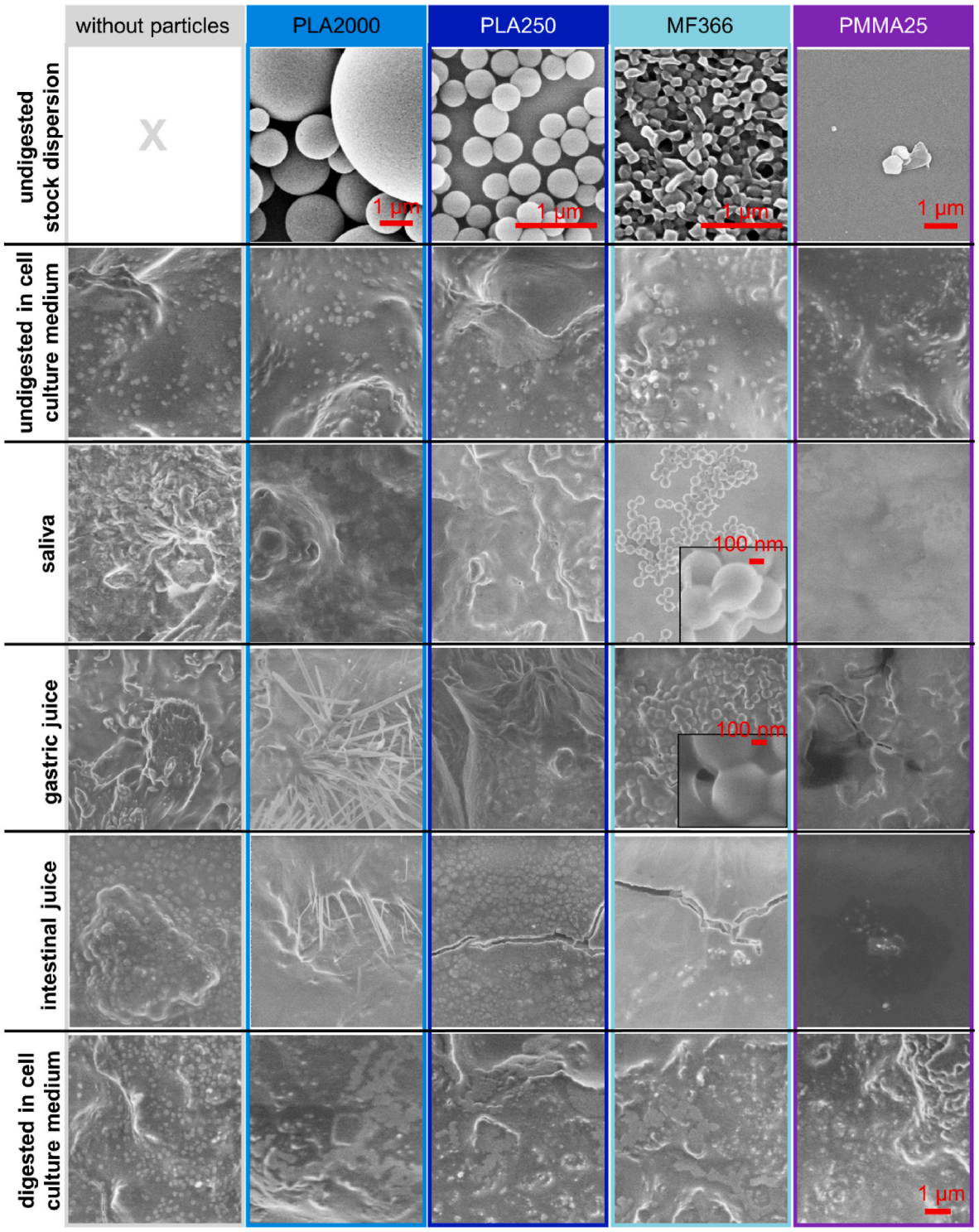

Fig. 6. Scanning Electron Microscopy (SEM) images of undigested plastic particles (stock dispersions, first row), undigested particles in cell culture medium (second row), digested particles taken at different stages of the *in vitro* digestion (saliva stage (third row), gastric stage (forth row), intestinal stage (fifth row)), and after complete digestion in cell culture medium (last row). Controls without particles are presented in the first column for comparison. A small amount of the sample was dropped on silica wafers, dried at room temperature and immediately analyzed.

$$g_{1,np}(\tau) = a_{np} e^{-\tau/\tau_{np}}$$

and aggregates thereof by

$$g_{1,agg}(\tau) = a_{agg} e^{-\tau/\tau_{agg}}$$

The $a_{1,np}$ and $a_{1,agg}$ are amplitudes, $\tau_{1,np}$ and $\tau_{1,agg}$ are decay times. The hydrodynamic diameter of species i (primary particle and aggregate, respectively) is then given as

$$D_{h,i} = \frac{k_B T q^2 \tau_i}{3\pi\eta}$$

where is k_B is the Boltzmann constant, T is the temperature of 296.15 K,

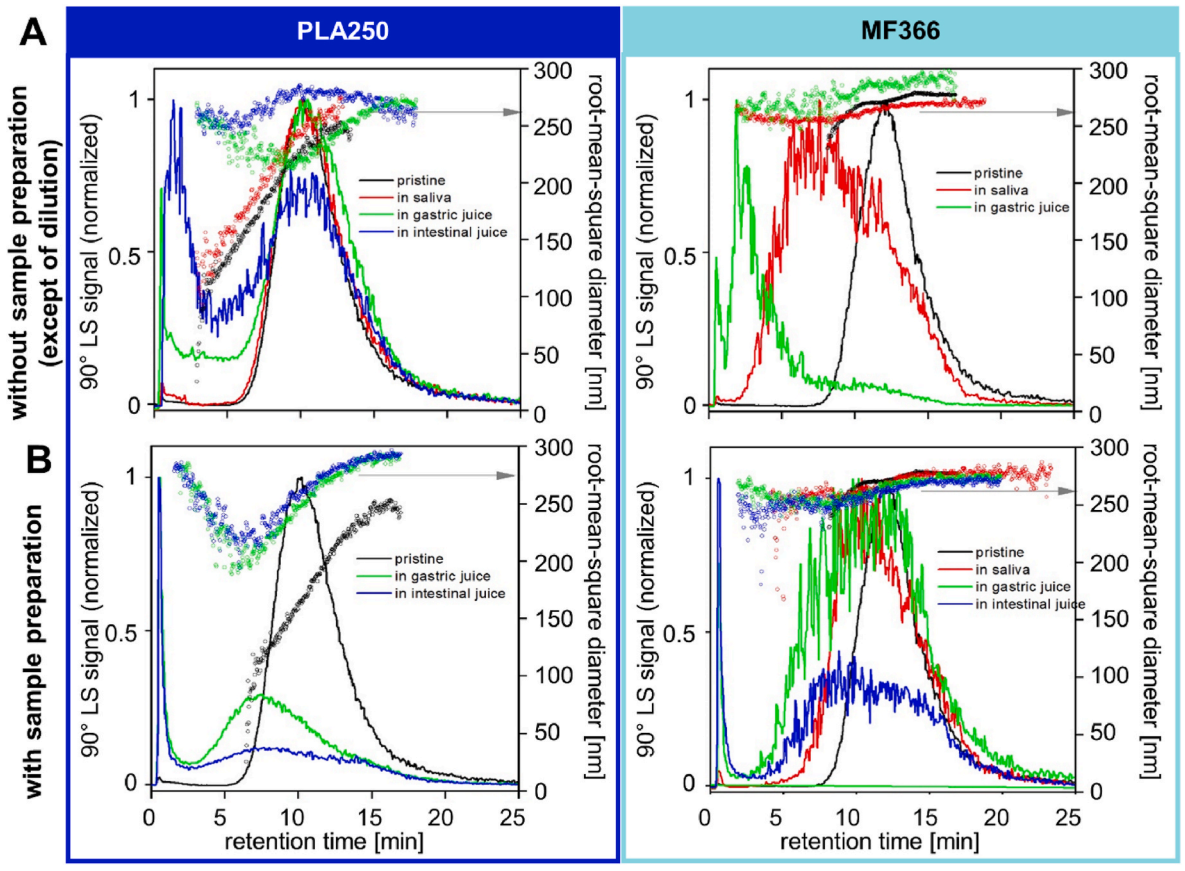

C

	PLA250			MF366			Control (digestion fluids)		
	Z-average	PDI	Derived CR (kcps)	Z-average	PDI	Derived CR (kcps)	Z-average	PDI	Derived CR (kcps)
pristine	277 ±8	0.08 ±0.04		417 ± 2	0.05 ±0.04				
saliva	289 ±7	0.21 ±0.03	1210 ±20	1118 ±127	0.36 ±0.02	15646 ± 683	830 ± 90	0.61 ±0.04	546 ± 61
gastric juice	412 ±9	0.43 ±0.05	674 ±48	1361 ±347	0.78 ±0.08	2215 ±1311	485 ±102	0.68 ±0.18	245 ±19
intestinal juice	537 ±16	0.44 ±0.04	520 ±165	1088 ±257	0.76 ±0.22	1460 ±294	738 ± 209	0.51 ±0.11	538 ±36

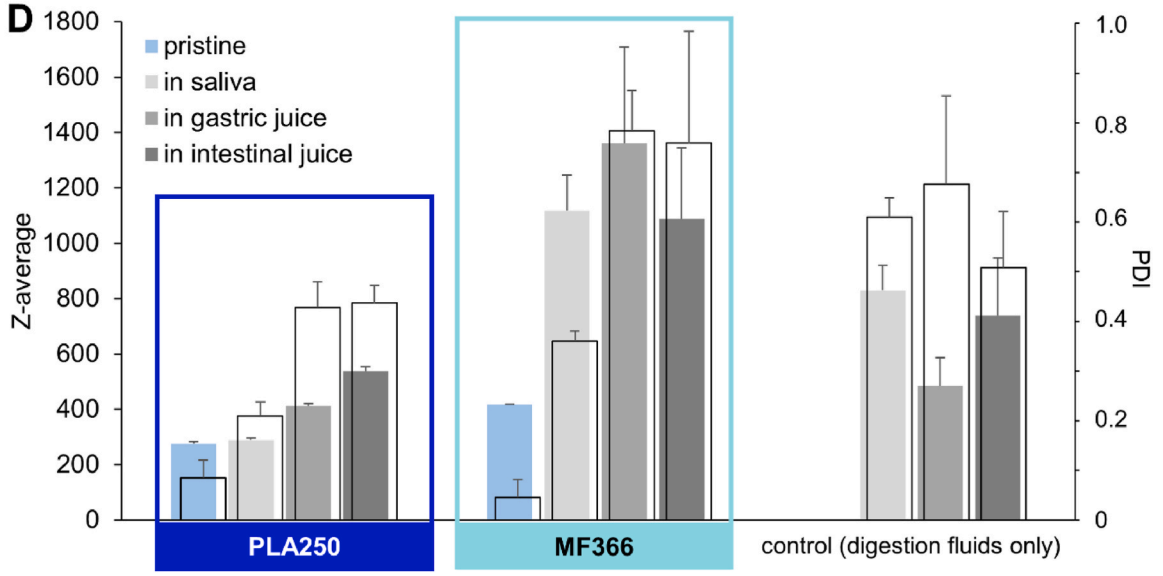

Fig. 7. AF4-MALS and DLS analysis of (un)digested PLA250 and MF366 particles. **A/B**: AF4-MALS without sample preparation (A) or with sample preparation (enzymatic treatment, B). **C/D**: DLS measurements depicted as table of results (C) and diagrams comparing z-average (no line, fill) and PDI (with line, no fill) of the two particles and the digestion fluids (saliva, gastric and intestinal juice). The results are presented as mean with SD, n = 3.

q is the scattering vector of 0.0180 nm^{-1}, η is the viscosity of 1.3147 mPa s (ca 41% higher than water (Poon, 2022)).

The experimental data of $g_{1s}(\tau)$ were derived from the experimental intensity correlation function data $G_{2s}(\tau)$ (see Fig. S3 and associated explanations). Next, a curve fit of $g_{1s}(\tau)$ of cell culture medium was performed providing fit parameters of $a_1 = 0.3449$, $a_2 = 0.4856$, $a_3 = 0.1507$, $t_1 = 4.79 \times 10^{-05}$ s, $t_2 = 1.93 \times 10^{-4}$ s, $t_3 = 2.54 \times 10^{-3}$ s (see Fig. S4). These relaxation times correspond to hydrodynamic diameters of $D_{h1} = 5.1$ nm, $D_{h2} = 20.6$ nm and $D_{h3} = 272$ nm. Without going into detail about the underlying structures, these quantities represent the complex composition of cell culture medium. One can certainly debate whether the composition of cell culture medium is indeed trimodal, or if instead a single broad distribution may be more realistic. Such distinction is not relevant, since $g_{1s}(\tau)$ is kept constant in further evaluation. It is of interest to note that the $g_{1s}(\tau)$ of blood serum was also best interpreted by the presence of a trimodal distribution with D_h-values of approximately 6–10, 34 to 60, and 140–400 nm (Rausch et al., 2010). However, this similarity between blood serum and the applied cell culture medium may be pure coincidence.

With the already known D_h-values of the pristine particles, the number of free fit parameters can be reduced by utilizing $\tau_{np} = (3\pi\eta D_h)/(k_B T q^2)$. Therefore, the remaining four free fit parameters of $g_1(\tau)$ are f, a_{np}, a_{agg} and τ_{agg}. Curve fits applying $g_1(\tau)$ are shown in Fig. 8 A (red solid lines). The individual contributions of $g_{1,s}(\tau)$, $g_{1,np}(\tau)$ and $g_{1,agg}(\tau)$ are provided for inspection. The characteristics of the data are well represented by the fit curves, even if, as expected, the curve fits with only four fit parameters are not perfect. But limiting the number of fit parameters to as few as possible avoids overfitting. When viewing the curves, it is obvious that the amplitude of $g_{1,agg}(\tau)$ is large for all the samples. Also, the $D_{h,agg}$-values of about 2.7×10^4 nm (PLA2000), 3.0×10^4 nm (PLA250), 2.1×10^3 nm (MF366) and 1.6×10^3 nm (PMMA25) are large. This indicates that a high number of particles are present in aggregated form (see upper left panel in Fig. 8 B).

For deeper insight, the number ratio of primary particles to aggregates is presented in Fig. 8 B. The scattering amplitude $a(D,q)$ is a measure for the number concentration n of the particles and for simplicity a spherical shape for the non-aggregated particles and their aggregates is assumed. For spherical particles with a diameter D_h and a scattering vector q applies

$$n \propto \frac{a(D,q)}{V(D)\,\Phi(D,q)}$$

With the volume of one particle $V(D) = \pi D^3/6$ and a scattering amplitude

$$\Phi(D,q) = 3\left[\sin\left(\frac{q\,D}{2}\right) - \frac{qD}{2}\cos\left(\frac{q\,D}{2}\right)\right]\left(\frac{q\,D}{2}\right)^{-3}$$

one obtains

$$n \propto \frac{2\,a(D,q)\left(\frac{q\,D}{2}\right)^3}{\pi D^3\left[\sin\left(\frac{q\,D}{2}\right) - \frac{qD}{2}\cos\left(\frac{q\,D}{2}\right)\right]}$$

The relative number of primary particles and the relative number of aggregates was calculated as $n_{np,rel} = n_{np}/(n_{np} + n_{agg})$ and $n_{agg,rel} = n_{agg}/(n_{np} + n_{agg})$. Note that absolute number densities, e.g. in units of mol/L are not available because the proportionally constant between n and $[a(D,q)]/[V(D)\,\Phi(D,q)]$ is unknown. Nevertheless, relative values are also meaningful. Thus, $n_{np,rel} = 47\%$ and $n_{agg,rel} = 53\%$ for PLA2000, 99% and 1% for PLA250, 68% and 32% for MF366 and 99% and 1% for PMMA25 are obtained (see right-hand panel of Fig. 8 B for comparison). These values show that the number concentration of non-aggregated particles is still much larger than that of the aggregates for the two smaller particles PLA250 and PMMA25. By contrast, $n_{np,rel}$ and $n_{agg,rel}$ are similar for the larger particles PLA2000 and MF366. This difference could be explained by the fact that the smaller particles have a considerably higher Brownian motion than the larger ones and are thus less prone to aggregation during the digestion process.

What is further important to evaluate is how many primary particles an aggregate contains. This can be estimated by the ratio of the volume of an aggregate to the volume of a primary particle $v_{agg}/v_{np} = D^3_{h,agg}/D^3_{h,np}$. We determined $v_{agg}/v_{np} = 9.4 \times 10^2$ for PLA2000, 1.3×10^6 for PLA250, 1.3×10^2 for MF366 and 3.1×10^4 for PMMA25 (see lower left panel of Fig. 8 B). These values illustrate that in all cases an aggregate contains a very high number of primary particles. In tendency, the smaller the primary particles, the more primary particles the aggregates contain. Lastly, it is of interest to see how high the volume fractions of the aggregates are in relation to the total plastics. The ratios of the total volume of aggregates to the total volume of particles was calculated as

$$v_{agg,rel} = \left(n_{agg} v_{agg}\right) / \left(n_{np} v_{np} + n_{agg} v_{agg}\right)$$

The calculated values of $v_{agg,rel}$ are 99% (PLA2000), 99% (PLA250), 98% (MF366) and 99% (PMMA25) (see right panel of Fig. 8 B). The large $v_{agg,rel}$-values demonstrate that, in contrast to the number fractions, the predominant volume fraction of the particles is present in form of aggregates.

Taken together, for all digested particle species, a certain aggregation was observable in the intestinal fluid diluted with cell culture medium. Thereof, both PLA particle species showed the highest fraction of aggregation, followed by PMMA and MF particles. PLA250 showed the largest aggregate size and also the highest size ratio between aggregates and primary particles. Even number-based, PLA250 led to predominantly aggregated particles, in contrast to PLA2000, where number-based aggregates and primary particles show an almost equal distribution. MF and PMMA particles generated smaller aggregates, which however also represent volume-based the vast majority of the particles in the digested intestinal juice samples.

4. Discussion and conclusion

Human exposure to micro- and nanoplastics is considered certain, due to the constantly increasing particle burden in the environment. Although research on this topic has increased significantly in recent years, no risk assessment is yet possible due to still existing data gaps. The complexity of plastic particles in terms of their materials, sizes, shapes, and surfaces aggravates a comprehensive risk characterization. Orally ingested particles need to pass digestive fluids (saliva, gastric and intestinal juice) before they can cross the intestinal barrier, and digestive fluids may affect particle characteristics and therefore change their systemic uptake. In most *in vitro* experiments using models of the intestinal barrier, pristine particles are applied (World Health Organization, 2022). Thus, the impact of the digestive process on plastic particles is still largely unknown (Toto et al., 2022). To close this knowledge gap, we have analyzed the changes of four different food-relevant plastic polymers in micro-, submicro- and nanometer ranges (PLA2000, PLA250, MF366, and PMMA25) during and after artificial digestion. We further investigated uptake and transport of these particles, compared to the undigested ones, as well as the toxicological impact based on the intestinal *in vitro* model Caco-2.

After performing the artificial digestion procedure, the particles and digestion fluids were analyzed for cytotoxic effects on differentiated Caco-2 cells using the MTT assay and the xCELLigence® system. From former artificial digestion experiments, it is known that the presence of intestinal fluid in the cell culture experiments alone can lead to a certain toxicity, especially at a dilution of 1:10 or less in cell culture medium (Sieg et al., 2020). Moreover, it can enhance the toxic effects of other substances. Consistently, in this study, intestinal fluid at the dilution of 1:10 led to a slight decrease of cell viability (Fig. 2 A). Regarding the

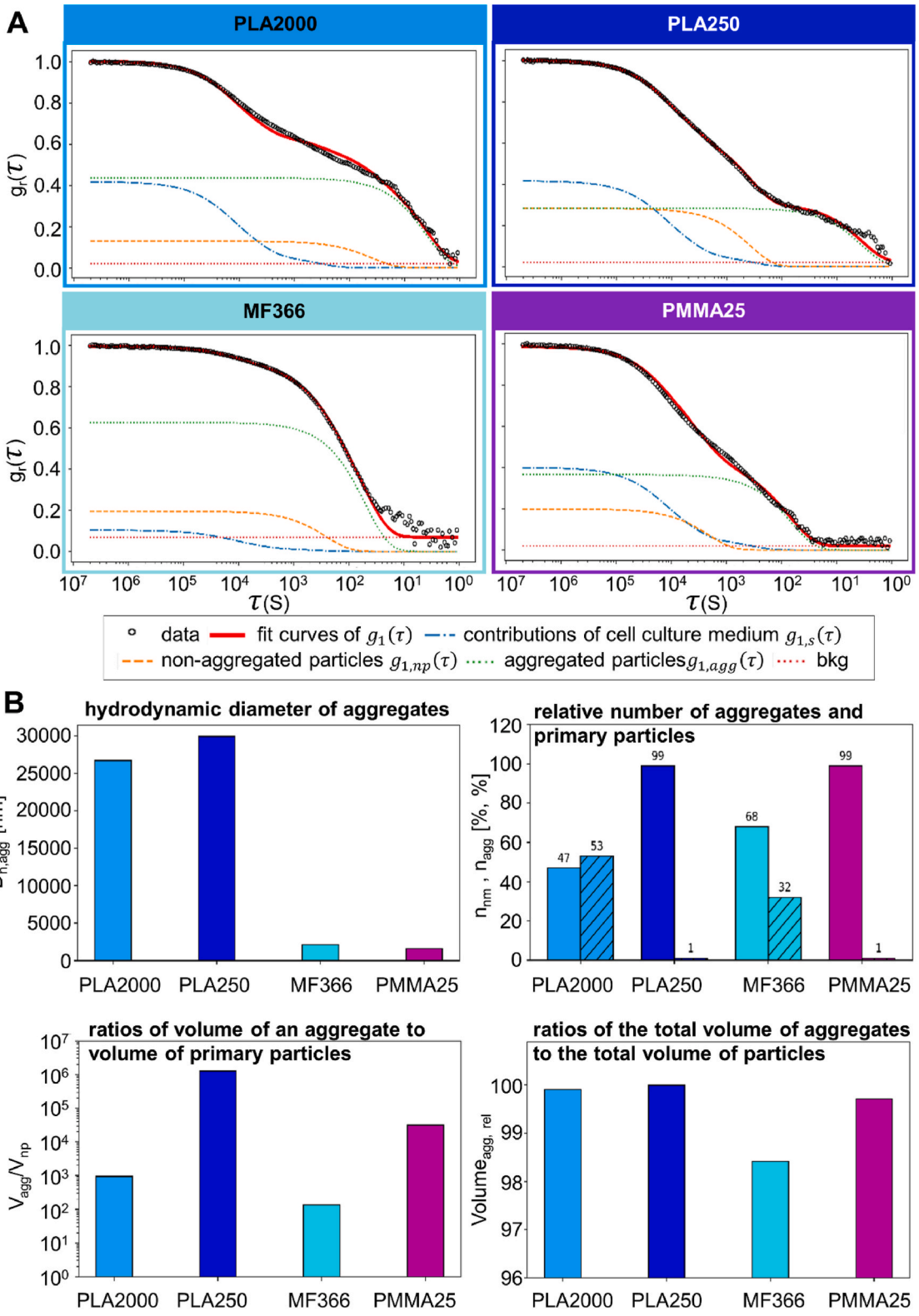

Fig. 8. DLS results of PLA200, PLA250, MF366 and PMMA25 after artificial digestion and dilution 1 to 99 (v/v) in cell culture medium (DMEM + 10 % FCS + 1 % P/S). **A:** Field autocorrelation data of digested particles PLA2000, PLA250, MF366 and PMMA25 (circles) and fit curves of $g_1(\tau)$ (red solid lines). The contributions of cell culture medium $g_{1,s}(\tau)$, the non-aggregated particles $g_{1,np}(\tau)$ and aggregated particles $g_{1,agg}(\tau)$ are displayed. **B:** Characteristics of the particles after digestion. Upper left panel: hydrodynamic diameter of aggregates $D_{h,agg} = 2.7 \times 10^4$ nm (PLA2000), 3.0×10^4 nm (PLA250), 2.1×10^3 nm (MF366) and 1.6×10^3 nm (PMMA25). Upper right panel: Relative number of primary particles and aggregates are $n_{np,rel} = 47\%$ and $n_{agg,rel} = 53\%$ (PLA2000), 99% and 1% (PLA250), 68% and 32% (MF366, 99% and 1% (PMMA25). Lower left panel: Ratios of volume of an aggregate to volume of primary particles $v_{agg}/v_{np} = 9.4 \times 10^2$ for PLA2000, 1.3×10^6 for PLA250, 1.3×10^2 for MF366 and 3.1×10^4 for PMMA250. Lower right panel: ratios of the total volume of aggregates to the total volume of particles $v_{agg,rel}$ are 99% (PLA2000), 99% (PLA250), 98% (MF366) and 99% (PMMA25). (For interpretation of the references to colour in this figure legend, the reader is referred to the Web version of this article.)

particle samples, only the MF366 particles led to a slightly increased cytotoxicity when diluted 1:10 in cell culture medium, even when normalized to the digestion controls (Fig. 2 B). For comparison, other groups observed a negative impact on the viability of proliferating (Li et al., 2023) and differentiated (Walczak et al., 2015) Caco-2 cells after exposure to digested 50 nm PS particles. Li et al. further reported that food matrices like carbohydrates, protein or fat could have an enhancing impact on cell viability (Li et al., 2023). Nevertheless, we did not observe cytotoxicity with the other applied plastic materials. The particles mostly remained deposited inside the cells as proven by fluorescence microscopy, and did not cause toxic effects. Taken together, only a very limited impact on cell viability was observed for the artificially digested particle species in this study.

For the *in vitro* translocation studies, a final dilution of the digested particles of 1:20 in cell culture medium was chosen as a non-cytotoxic concentration. The uptake and transport of digested particles was analyzed and compared to undigested particles. Our results show that, compared to undigested particles, the relative cellular uptake and interaction of the digested particles with the Caco-2 cells decreased after artificial digestion (Fig. 4 B). This can be related to the strong agglomeration of all particles with the organic matter of the intestinal fluid, as shown in SEM images. This attachment might result in a decreased cellular uptake, because less primary particles are available to the cells. In addition, the confocal microscope images (and their quantification) only reflect snapshots of the cellular interaction after 24 h and certainly do not reflect the underlying dynamics of the translocation process. This might lead to over- or underestimated results. The agglomeration behavior of the artificially digested plastic was analyzed by AF4-MALS and DLS, which revealed interesting results regarding particle behavior, dependent on the polymer. Analyzing small plastic particles in a complex matrix like digestion fluids is generally challenging. DLS analysis is interfered with by other light-scattering entities in the fluids like proteins. A special fitting procedure can allow to distinguish between the matrix contributions assigned to the particles and the medium/organic matter. AF4 allows the separation by size and reduces this effect. The disadvantage of AF4 is that the elution behavior of the particles can be influenced by the matrix as demonstrated also by our results. Relying on retention times for determination of particle sizes would lead to erroneous results. Coupling with MALS allows direct determination of particle sizes and identification of non-ideal elution behavior. All particles showed agglomeration in the intestinal fluid, but there were differences in agglomerated fractions as well as in the sizes of the agglomerates. PLA2000 and PLA250 particles formed the largest agglomerates by far, compared to MF366 and PMMA25. In a previous study, the PLA particles were characterized to be rather hydrophobic, while MF and PMMA had more hydrophilic properties (Paul et al., 2022), which might influence the aggregation behavior. However, both PLA materials showed also differences between the agglomerated fractions. Regarding the polydisperse PLA2000, number-based a higher fraction of primary particles remained in the sample, while PLA250 was observed to be almost completely agglomerated. This agglomeration could be reasoned in the shape of the particles. PLA2000 was characterized more spherical, while the characterization of pristine PLA250 showed almost spherical, but more strongly attached irregular agglomerates in electron microscopy (Paul et al., 2022). The results can be compared to previous studies we did in our group. Stock et al. artificially digested PS, polyethylene (PE), polypropylene, polyvinyl chloride and polyethylene terephthalate microplastic particles (Stock et al., 2020). They could show by using SEM that in intestinal fluid, especially PS microparticles showed a strong agglomeration, as it was also the case for our test particles. This agglomeration led to an increasing agglomerate size from saliva over stomach fluid to intestinal fluid. While in stomach fluid, mainly the low pH values lead to the lack of electrostatic stabilization; in the intestinal juice the presence of organic matter fluid most likely leads to the agglomerate formation. Removal of the organic matter by peroxide digestion led to a disappearance of these large agglomerates, which proved that primary particle size does not change during digestion.

We further quantified particle transport through the Caco-2 epithelium for all test particles by applying fluorescence measurements and microscopy. Compared to the undigested particles, the digested particles appear to have a slightly increased transport rate (Figs. 4 and 5). This difference might be explained by the presence of organic matter, which influences the ability of the particles to cross the epithelium. It is conceivable that even if digestion has caused particle agglomerates, the organic matrix facilitates the transport of the particles through the epithelium. Based on this assumption, it is in accordance with the reduced cellular interaction, as the particles remain within the cell layer for a shorter time period and are translocated more rapidly. A higher translocation of digested 50 nm PS (with surface functionalization) compared to undigested particles was also shown by Walczak et al. (2015). They applied the particles to a mucus-producing Caco-2/HT29-MTX co-culture model, and additionally reported an impact on protein corona amount and composition. Furthermore, the effects of the particles were dependent on surface functionalization (Walczak et al., 2015). Even though our particles had no surface functionalization, we could also show surface-dependent effects, presumably based on hydrophobicity. Anyway, the number of current publications dealing with artificial digestion of micro- and nanoplastics followed by an incubation on cellular models is still rare. Furthermore, different study designs regarding particle concentration, incubation time, selected polymers and particle sizes as well as cellular models and endpoints limit their comparability. For example, Li et al. have focused on the impact of food components like bovine serum albumin, starch and glyceryl trioleate on digested 50 nm PS particles. They exposed proliferating Caco-2 cells to digested particles for 72 h and quantified that the uptake rate was higher for digested particles. Nevertheless, they did not investigate translocation of particles. When adding food matrices, the uptake was enhanced (Li et al., 2023). Another group digested 25 nm, 100 nm and 1000 nm PS particles and applied them to a co-culture model of Caco-2/HT29-MTX/Raji B (DeLoid et al., 2021, 2022). They reported less than 1.5 % transport of the PS particles after 4 h exposure to the cellular model. When discussing the data, it needs to be considered that incubation time was only 4 h, the cell culture medium differed as that it did not contain FCS, and the authors did not compare their results to undigested particles. In another publication, the researchers focused on the influence of PE particles on the digestion process of high fat food. The presence of 400 μg/mL PE nanoparticles (approx. 100 nm) increased fat digestion by 33 % and fat absorption by 145 % after 2 h exposure in the co-culture model (DeLoid et al., 2022). By contrast, Tan et al. investigated the influence of PS, PE, polyethylene terephthalate, polyvinyl chloride and poly(lactic-*co*-glycolic acid) on the enzymatic lipid digestion in the digestive fluids. They quantified a reduced lipid digestion, independent of particle size (Tan et al., 2020). Another important aspect is the interaction of microplastic particles with microbiota, as investigated by e.g. Huang et al. (2021) and Fournier et al., 2021, 2023. Moreover, the release of environmental chemicals and metals from polypropylene, PE, PS, or polyvinyl chloride particles, as investigated by Peters et al. (2022), in a similar artificial digestion system, needs to be considered (Peters et al., 2022).

To sum up, the number of published studies regarding the impact of artificial digestion on particles recently increased. However, only prominent materials like PS or PE have been analyzed under various aspects, but often using non-comparable experimental settings. This study adds up information on micro-, submicro- and nanoplastic particles made of PLA, MF and PMMA. The herein presented results show a possible impact of the digestion process on particle characteristics and interaction with differentiated Caco-2 cells. Although the artificial digestion did not destruct or change the size and shape of primary plastic particles, there were big differences in the agglomeration behavior and the agglomerate size, dependent of polymer type, particle size and surface properties of the test particles. This further had an impact on

particle uptake and translocation across the Caco-2 cell monolayer. Since consumers are never exposed to pristine particles in real life, the presence and influence of digestive fluids should be considered in future research on the oral ingestion of micro-, submicro- and nanoplastic particles.

Availability of data and materials

All data generated or analyzed during this study are included in this published article and its supplementary information files.

Funding

This project was funded by the German Federal Institute for Risk Assessment, Germany (projects 1322-782 and 1329–003-1222214).

CRediT authorship contribution statement

Maxi B. Paul: Conceptualization, Data curation, Formal analysis, Investigation, Methodology, Software, Validation, Visualization, Writing – original draft, Writing – review & editing. **Linda Böhmert:** Conceptualization, Data curation, Validation, Visualization, Writing – original draft, Writing – review & editing. **Andreas F. Thünemann:** Data curation, Formal analysis, Investigation, Methodology, Software, Validation, Visualization, Writing – original draft. **Katrin Loeschner:** Data curation, Formal analysis, Investigation, Methodology, Software, Validation, Visualization, Writing – original draft. **Lucas Givelet:** Data curation, Investigation, Methodology, Validation, Writing – original draft. **Christoph Fahrenson:** Data curation, Formal analysis, Methodology, Software, Validation, Visualization, Writing – original draft. **Albert Braeuning:** Conceptualization, Funding acquisition, Supervision, Writing – original draft, Writing – review & editing. **Holger Sieg:** Conceptualization, Data curation, Formal analysis, Funding acquisition, Investigation, Methodology, Project administration, Resources, Software, Supervision, Writing – original draft, Writing – review & editing.

Declaration of competing interest

The authors declare that they have no known competing financial interests or personal relationships that could have appeared to influence the work reported in this paper.

Data availability

Data will be made available on request.

Acknowledgements

The authors thank Marén Schlief for technical assistance. We further would like to thank Maximilian Ebisch, Petra Fengler and Tina Rybak for their help in performing the artificial digestion of the particles.

Appendix A. Supplementary data

Supplementary data to this article can be found online at https://doi.org/10.1016/j.fct.2023.114423.

References

Abdelkhaliq, A., Van Der Zande, M., Undas, A.K., Peters, R.J., Bouwmeester, H., 2020. Impact of in vitro digestion on gastrointestinal fate and uptake of silver nanoparticles with different surface modifications. Nanotoxicology 14, 111–126.

Bitou, N., Ninomiya, M., Tsujita, T., Okuda, H., 1999. Screening of lipase inhibitors from marine algae. Lipids 34, 441–445.

Böhmert, L., Girod, M., Hansen, U., Maul, R., Knappe, P., Niemann, B., Weidner, S.M., Thünemann, A.F., Lampen, A., 2014. Analytically monitored digestion of silver nanoparticles and their toxicity on human intestinal cells. Nanotoxicology 8, 631–642.

Caldwell, J., Taladriz-Blanco, P., Lehner, R., Lubskyy, A., Ortuso, R.D., Rothen-Rutishauser, B., Petri-Fink, A., 2022. The micro-, submicron-, and nanoplastic hunt: a review of detection methods for plastic particles. Chemosphere 293, 133514.

Correia, M., Loeschner, K., 2018. Detection of nanoplastics in food by asymmetric flow field-flow fractionation coupled to multi-angle light scattering: possibilities, challenges and analytical limitations. Anal. Bioanal. Chem. 410, 5603–5615.

Da Silva Brito, W.A., Mutter, F., Wende, K., Cecchini, A.L., Schmidt, A., Bekeschus, S., 2022. Consequences of nano and microplastic exposure in rodent models: the known and unknown. Part. Fibre Toxicol. 19, 28.

Deloid, G.M., Cao, X., Bitounis, D., Singh, D., Llopis, P.M., Buckley, B., Demokritou, P., 2021. Toxicity, uptake, and nuclear translocation of ingested micro-nanoplastics in an in vitro model of the small intestinal epithelium. Food Chem. Toxicol. 158, 112609.

Deloid, G.M., Cao, X., Coreas, R., Bitounis, D., Singh, D., Zhong, W., Demokritou, P., 2022. Incineration-generated polyethylene micro-nanoplastics increase triglyceride lipolysis and absorption in an in vitro small intestinal epithelium model. Environ. Sci. Technol. 56, 12288–12297.

EFSA, 2016. Presence of microplastics and nanoplastics in food, with particular focus on seafood. EFSA J. 14, e04501.

Eyerer, P., 2010. Plastics: Classification, Characterization and Economic Data. *Polymers - Opportunities and Risks I: General and Envrionmental Aspects*.

Fournier, E., Etienne-Mesmin, L., Grootaert, C., Jelsbak, L., Syberg, K., Blanquet-Diot, S., Mercier-Bonin, M., 2021. Microplastics in the human digestive environment: a focus on the potential and challenges facing in vitro gut model development. J. Hazard Mater. 415, 125632.

Fournier, E., Leveque, M., Ruiz, P., Ratel, J., Durif, C., Chalancon, S., Amiard, F., Edely, M., Bezirard, V., Gaultier, E., 2023. Microplastics: what happens in the human digestive tract? First evidences in adults using in vitro gut models. J. Hazard Mater. 442, 130010.

Frias, J., Pagter, E., Nash, R., O'connor, I., Carretero, O., Filgueiras, A., Viñas, L., Gago, J., Antunes, J., Bessa, F., 2018. Standardised protocol for monitoring microplastics in sediments. Deliverable 4.2.

Gesamp, 2015. Sources, fate and effects of microplastics in the marine environment: a global assessement. In: KERSHAW, P.J. (Ed.), 4 Albert Embankment, London SE1 7SR. International maritime organization.

Gray, S.P., Billings, J.A., 1983. Kinetic assay of human pepsin with albumin Bromphenol blue as substrate. Clin. Chem. 29, 447–451.

Hartmann, N.B., Hüffer, T., Thompson, R.C., Hassellöv, M., Verschoor, A., Daugaard, A. E., Rist, S., Karlsson, T., Brennholt, N., Cole, M., Herrling, M.P., Hess, M.C., Ivleva, N. P., Lusher, A.L., Wagner, M., 2019. Are we speaking the same language? Recommendations for a definition and categorization framework for plastic debris. Environ. Sci. Technol. 53, 1039–1047.

Huang, W., Yin, H., Yang, Y., Jin, L., Lu, G., Dang, Z., 2021. Influence of the co-exposure of microplastics and tetrabromobisphenol A on human gut: simulation in vitro with human cell Caco-2 and gut microbiota. Sci. Total Environ. 778, 146264.

Kästner, C., Lampen, A., Thünemann, A.F., 2018. What happens to the silver ions?–Silver thiocyanate nanoparticle formation in an artificial digestion. Nanoscale 10, 3650–3653.

Kästner, C., Lichtenstein, D., Lampen, A., Thünemann, A.F., 2017. Monitoring the Fate of Small Silver Nanoparticles during Artificial Digestion A Physicochemical and Engineering Aspects.

Khan, A., Jia, Z.Q., 2023. Recent insights into uptake, toxicity, and molecular targets of microplastics and nanoplastics relevant to human health impacts. iScience 26.

Lea, T., 2015. Caco-2 cell line. In: Verhoeckx, K., Cotter, P., Lopez-Exposito, I., Kleiveland, C., Lea, T., Mackie, A., Requena, T., Swiatecka, D., Wichers, H. (Eds.), The Impact of Food Bioactives on Health: in Vitro and Ex Vivo Models. Cham (CH).

Li, Z., Huang, Y., Zhong, Y., Liang, B., Yang, X., Wang, Q., Sui, H., Huang, Z., 2023. Impact of food matrices on the characteristics and cellular toxicities of ingested nanoplastics in a simulated digestive tract. Food Chem. Toxicol., 113984

Lichtenstein, D., Ebmeyer, J., Knappe, P., Juling, S., Böhmert, L., Selve, S., Niemann, B., Braeuning, A., Thünemann, A.F., Lampen, A., 2015. Impact of food components during in vitro digestion of silver nanoparticles on cellular uptake and cytotoxicity in intestinal cells. Biol. Chem. 396, 1255–1264.

Liu, S., Wu, X., Gu, W., Yu, J., Wu, B., 2020. Influence of the digestive process on intestinal toxicity of polystyrene microplastics as determined by in vitro Caco-2 models. Chemosphere 256, 127204.

Oomen, A., Rompelberg, C., Bruil, M., Dobbe, C., Pereboom, D., Sips, A., 2003. Development of an in vitro digestion model for estimating the bioaccessibility of soil contaminants. Arch. Environ. Contam. Toxicol. 44, 281–287.

Paul, M.B., Böhmert, L., Hsiao, I.L., Braeuning, A., Sieg, H., 2023. Complex intestinal and hepatic in vitro barrier models reveal information on uptake and impact of micro-, submicro- and nanoplastics. Environ. Int. 179, 108172.

Paul, M.B., Fahrenson, C., Givelet, L., Herrmann, T., Loeschner, K., Böhmert, L., Thünemann, A.F., Braeuning, A., Sieg, H., 2022. Beyond microplastics - investigation on health impacts of submicron and nanoplastic particles after oral uptake in vitro. Microplastics and Nanoplastics 2, 16.

Peters, R., De Jong, N., De Haan, L., Wright, S., Bouwmeester, H., 2022. Release and intestinal translocation of chemicals associated with microplastics in an in vitro human gastrointestinal digestion model. Microplastics and Nanoplastics 2, 1–21.

Peters, R., Kramer, E., Oomen, A.G., Herrera Rivera, Z.E., Oegema, G., Tromp, P.C., Fokkink, R., Rietveld, A., Marvin, H.J., Weigel, S., 2012. Presence of nano-sized silica during in vitro digestion of foods containing silica as a food additive. ACS Nano 6, 2441–2451.

Poon, C., 2022. Measuring the density and viscosity of culture media for optimized computational fluid dynamics analysis of in vitro devices. J. Mech. Behav. Biomed. Mater. 126.

Rausch, K., Reuter, A., Fischer, K., Schmidt, M., 2010. Evaluation of nanoparticle aggregation in human blood serum. Biomacromolecules 11, 2836–2839.
Ritchie, H., Roser, M., 2022. Plastic Pollution. *Our World In Data*.
Sieg, H., Kästner, C., Krause, B., Meyer, T., Burel, A., Böhmert, L., Lichtenstein, D., Jungnickel, H., Tentschert, J., Laux, P., 2017. Impact of an artificial digestion procedure on aluminum-containing nanomaterials. Langmuir 33, 10726–10735.
Sieg, H., Krause, B.-C., Kästner, C., Böhmert, L., Lichtenstein, D., Tentschert, J., Jungnickel, H., Laux, P., Braeuning, A., Fessard, V., 2020. Cellular effects of in vitro-digested aluminum nanomaterials on human intestinal cells. ACS Appl. Nano Mater. 3, 2246–2256.
Stock, V., Fahrenson, C., Thuenemann, A., Dönmez, M.H., Voss, L., Böhmert, L., Braeuning, A., Lampen, A., Sieg, H., 2020. Impact of artificial digestion on the sizes and shapes of microplastic particles. Food Chem. Toxicol. 135, 111010.
Stock, V., Laurisch, C., Franke, J., Dönmez, M.H., Voss, L., Böhmert, L., Braeuning, A., Sieg, H., 2021. Uptake and cellular effects of PE, PP, PET and PVC microplastic particles. Toxicol. Vitro 70, 105021.
Tan, H., Yue, T., Xu, Y., Zhao, J., Xing, B., 2020. Microplastics reduce lipid digestion in simulated human gastrointestinal system. Environ. Sci. Technol. 54, 12285–12294.
Toto, B., Refosco, A., O'keeffe, M., Barkhald, O.H., Bronstad, A., Lied, G.A., Yadetie, F., Goksoyr, A., Kogel, T., Dierkes, J., 2022. Intestinal permeability and gene expression after polyethylene and polyamide microplastic ingestion in Wistar rats. Toxicol. Lett. 370, 35–41.
Toussaint, B., Raffael, B., Angers-Loustau, A., Gilliland, D., Kestens, V., Petrillo, M., Rio-Echevarria, I.M., Van Den Eede, G., 2019. Review of micro- and nanoplastic contamination in the food chain. Food Addit. Contam. Part A Chem Anal Control Expo Risk Assess 36, 639–673.
Versantvoort, C.H., Oomen, A.G., Van De Kamp, E., Rompelberg, C.J., Sips, A.J., 2005. Applicability of an in vitro digestion model in assessing the bioaccessibility of mycotoxins from food. Food Chem. Toxicol. 43, 31–40.
Voss, L., Hoché, E., Stock, V., Böhmert, L., Braeuning, A., Thünemann, A.F., Sieg, H., 2021. Intestinal and hepatic effects of iron oxide nanoparticles. Arch. Toxicol. 95, 895–905.
Voss, L., Saloga, P.E., Stock, V., Böhmert, L., Braeuning, A., Thünemann, A.F., Lampen, A., Sieg, H., 2019. Environmental impact of ZnO nanoparticles evaluated by in vitro simulated digestion. ACS Appl. Nano Mater. 3, 724–733.
Walczak, A.P., Fokkink, R., Peters, R., Tromp, P., Herrera Rivera, Z.E., Rietjens, I.M., Hendriksen, P.J., Bouwmeester, H., 2012. Behaviour of silver nanoparticles and silver ions in an in vitro human gastrointestinal digestion model. Nanotoxicology 7, 1198–1210.
Walczak, A.P., Kramer, E., Hendriksen, P.J., Helsdingen, R., Van Der Zande, M., Rietjens, I.M., Bouwmeester, H., 2015. In vitro gastrointestinal digestion increases the translocation of polystyrene nanoparticles in an in vitro intestinal co-culture model. Nanotoxicology 9, 886–894.
World Health Organization, 2022. Dietary and Inhalation Exposure to Nano- and Microplastic Particles and Potential Implications for Human Health. Geneva.

SUPPORTING INFORMATION

Influence of artificial digestion on characteristics and intestinal cellular effects of micro-, submicro- and nanoplastics

Maxi B. Paul[1], Linda Böhmert[1], Andreas F. Thünemann[2], Katrin Loeschner[3], Lucas Givelet[3] Christoph Fahrenson[4], Albert Braeuning[1], Holger Sieg[1]*

1 German Federal Institute for Risk Assessment, Department of Food Safety, Max-Dohrn-Str. 8-10, 10589 Berlin, Germany
2 Federal Institute for Materials Research and Testing (BAM), Division Synthesis and Scattering of Nanostructured Materials , Unter den Eichen 87, 12205 Berlin, Germany
3 Technical University of Denmark, Research Group for Analytical Food Chemistry, Kemitorvet 201, 2800 Kgs. Lyngby, Denmark.
4 Technical University of Berlin, Center for Electron Microscopy (ZELMI), Straße des 17. Juni 135, 10623 Berlin, Germany.

*** Corresponding Author:**
Holger Sieg, German Federal Institute for Risk Assessment, Max-Dohrn Straße 8-10, 10589 Berlin, Germany. Phone: +49 (30) 18412-25102, E-Mail: holger.sieg@bfr.bund.de

Table S1: Overview of applied separation program for AF4 measurements

Step	Duration [min]	Mode	Cross flow start [mL/min]	Cross flow end [mL/min]
1	2	Elution	0.2	0.2
2	1	Focus		
3	2	Focus + injection		
4	10	Focus		
5	30	Elution	0.2	0.1

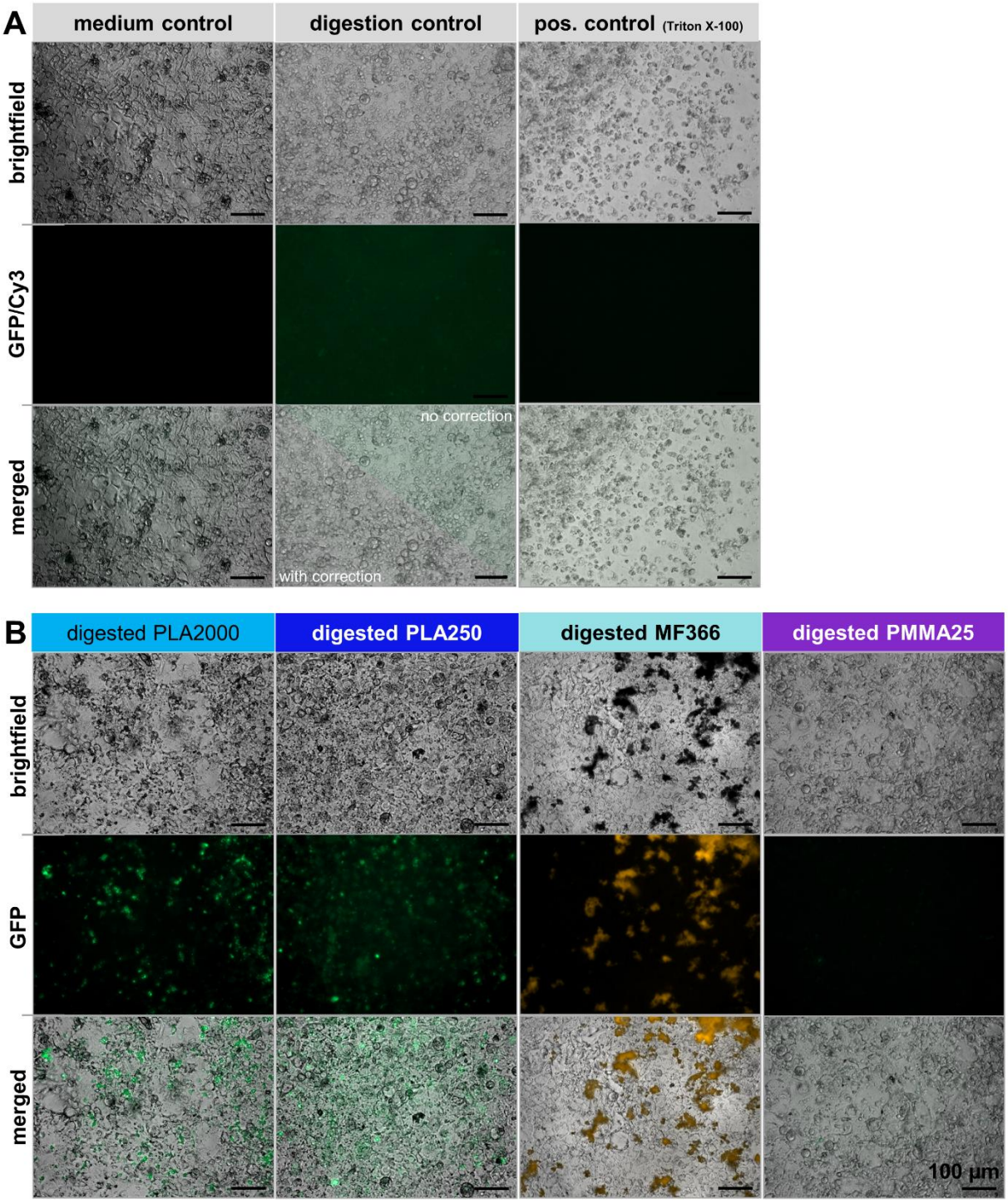

Figure S1: Representative fluorescence microscopy images of **A:** controls (medium, intestinal juice and Triton X-100 as positive control) and **B:** digested particles (PLA2000, PLA250, MF366 and PMMA25) incubated for 24 h on differentiated Caco-2 cells (1:20 dilution). The upper rows represent the brightfield channel, the middle row GPF or Cy3 channel (depending on particles fluorescence label, particles are shown in green or orange) and the lower row the merged channel. The intestinal juice had some intrinsic fluorescence, which was corrected in all figures of the digestested particles in order to emphasize particles present on/in the cells.

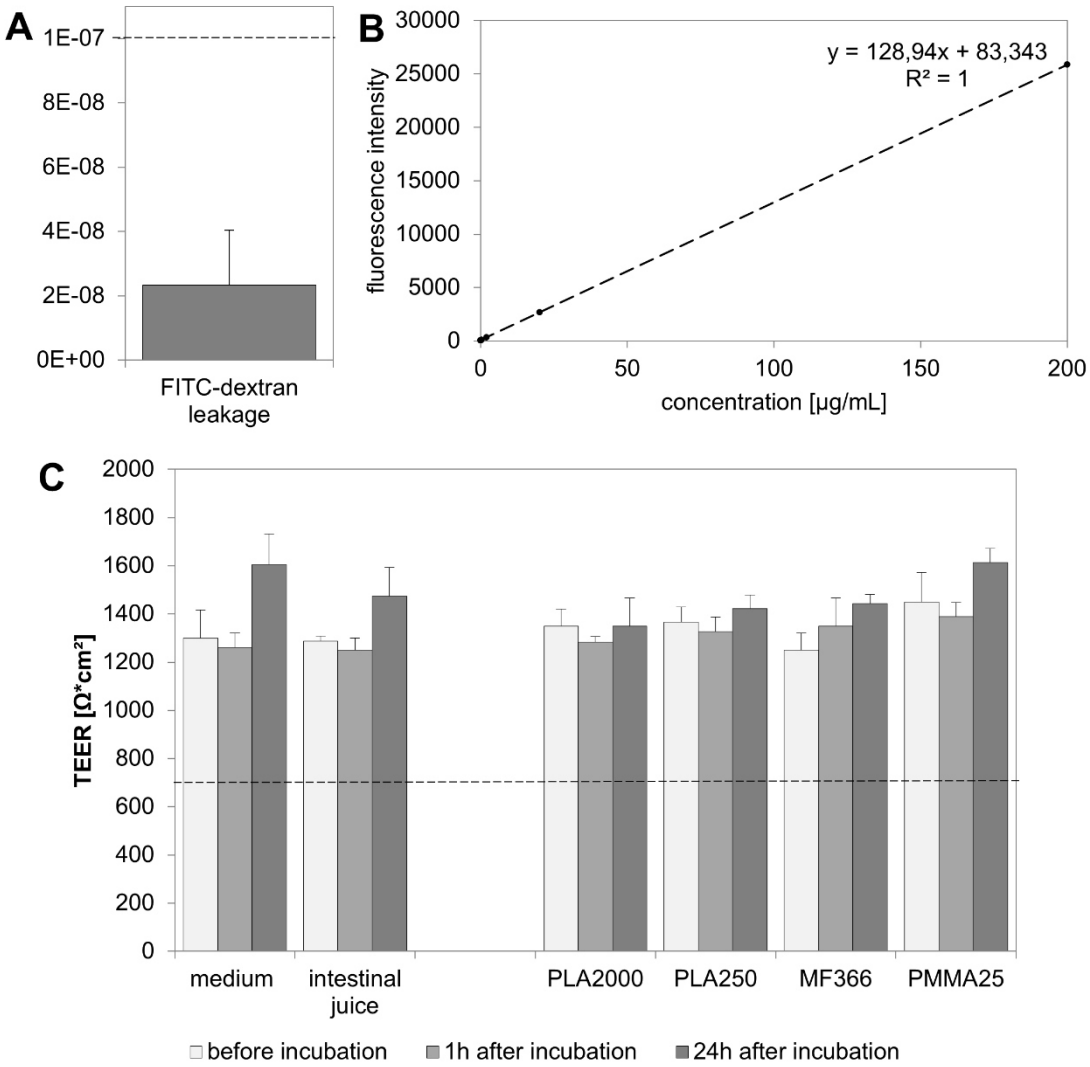

Figure S2: Barrier integrity measurements. **A**/**B** FITC-dextran leakage. **A** P_{app} value and standard deviation of the medium control quantified in the Caco-2 monoculture. All values were below the upper transport limit. n = 3. **B**. Representative standard curve. The formula of the trendline was used to calculate P_{app} values. **C** Mean TEER values and standard deviation of medium control, intestinal juice and the test particles PLA2000, PLA250, MF366, PMMA25 before, 1 h and 24 h after incubation with respective particles in the Caco-2 monoculture (n=3).

DLS of particles in cell culture medium

Estimation of the field autocorrelation function $g_1(\tau)$

Before applying the described data interpretation, it was necessary to extract the experimental field autocorrelation function $g_1(\tau)$ from the measured intensity autocorrelation function $\mathrm{G}_2(\tau)$. The functions are related by Finsy (Finsy, 1994):

$$G_2(\tau) = A + B\, g_1^2(\tau) + \epsilon(\tau)$$

where $\mathrm{G}_2(\tau)$ are the measured data, A is a background, B is an instrument factor and $\epsilon(\tau)$ is an unknown experimental uncertainty.

Adapting the recommendations of Finsy (Finsy, 1994), we determined $\mathrm{g}_1(\tau)$ in following four steps:

1. $G_2(\tau)$ decays to its background value A for large time delays, i.e., the baseline is approached by a measurement of $G_2(\tau)$ for large delay times. The background was estimated as $\lim_{\tau\to\infty} G_2(\tau)$
2. The background was subtracted as $\mathrm{G}_2(\tau) - \mathrm{A}$. In case negative values occurred, these were replaced with $|G_2 - A|$.
3. Estimation of B by fitting $\mathrm{G}_2(\tau) - \mathrm{A} \approx \mathrm{B}\, \mathrm{e}^{-2\frac{\tau}{\tau_0}}$ at small τ-values
4. Calculation of $\mathrm{g}_1(\tau) = \sqrt{(\mathrm{G}_2 - \mathrm{A})/\mathrm{B}}$

An illustration of the application of this procedure is provided for the pure cell culture medium exemplarily in Figure S4.

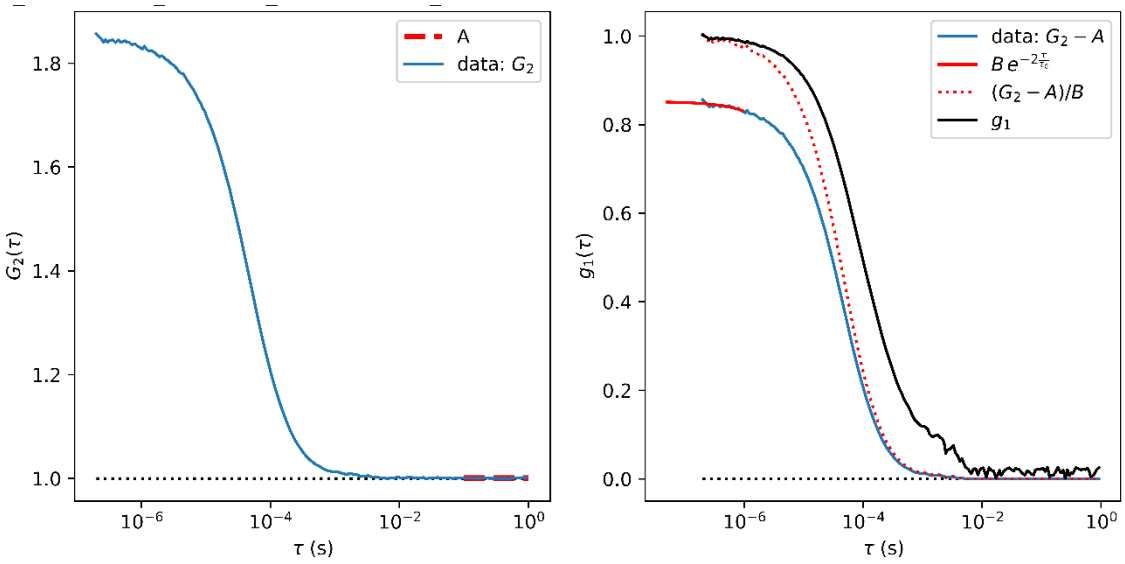

Figure S3: DLS of the cell culture medium and the estimation of $g_1(\tau)$ from $G_2(\tau)$. Left: Experimental $G_2(\tau)$-data of the cell culture medium (blue solid line) and the baseline *A* (red dashed line). Right: Experimental data after subtraction of the baseline $|G_2 - A|$ (blue solid line). Curve fit of $G_2(\tau) - A$ by $B\, e^{-2\frac{\tau}{\tau_0}}$ at small values of τ (red solid line). Calculated values of $(G_2 - A)/B$ (red dotted line) and $g_1(\tau) = \sqrt{(G_2 - A)/B}$ (black solid line).

Curve fit of the DLS data of the CCM

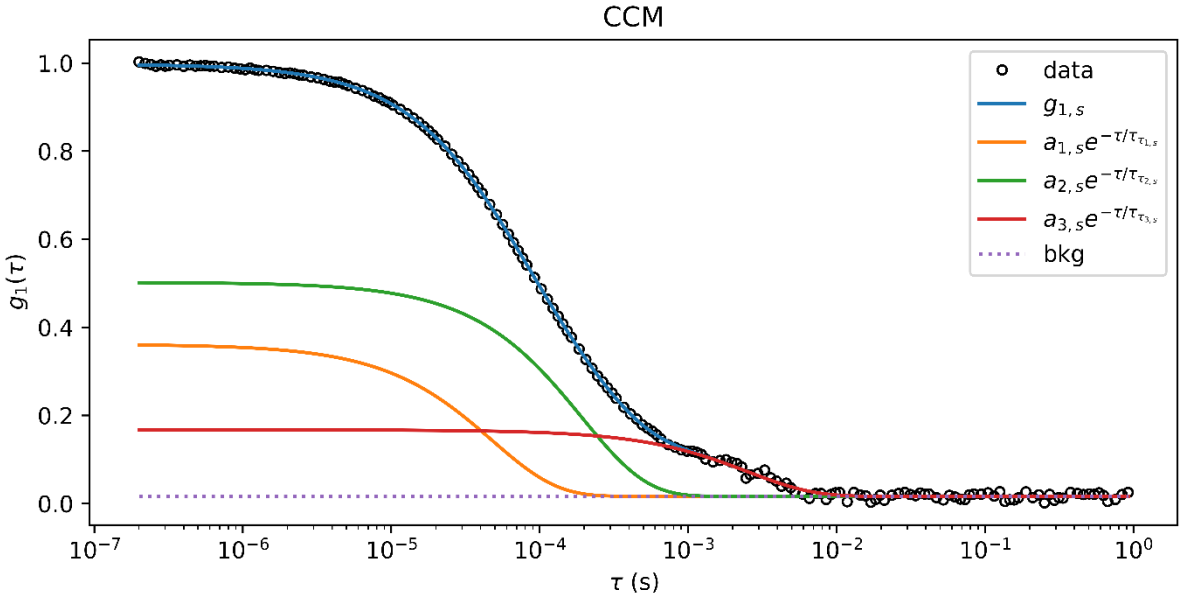

Figure S4: Experimental field autocorrelation data of the cell culture medium (circles) and its curve fit with $g_1(\tau)$ (blue solid line). The individual contributions to $g_1(\tau)$ are $a_{1,s}e^{-\tau/\tau_{\tau_{1,s}}}$ (orange line), $a_{2,s}e^{-\tau/\tau_{\tau_{2,s}}}$ (green line) and $a_{3,s}e^{-\tau/\tau_{\tau_{3,s}}}$ (red line). Fit parameters are $a_1 = 0.3449$, $a_2 = 0.4856$, $a_3 = 0.1507$, $t_1 = 4.79 \times 10^{-05}$ s, $t_2 = 1.93 \times 10^{-4}$ s, $t_3 = 2.54 \times 10^{-3}$ s. The relaxation times correspond to hydrodynamic diameters of $D_{h1} = 5.1$ nm, $D_{h2} = 20.6$ nm and $D_{h3} = 272$ nm.

References

FINSY, R. 1994. Particle Sizing by Quasi-Elastic Light-Scattering. *Advances in Colloid and Interface Science,* 52**,** 79-143.